

DOES THE BLAZAR GAMMA-RAY SPECTRUM HARDEN WITH INCREASING FLUX? - ANALYSIS OF NINE YEARS OF EGRET DATA.

GIRIDHAR NANDIKOTKUR^{1,2}, KEITH M. JAHODA², R. C. HARTMAN², R. MUKHERJEE³, P. SREEKUMAR⁴, M. BÖTTCHER⁵,
R. M. SAMBRUNA², AND JEAN H. SWANK²

Accepted for publication in ApJ

ABSTRACT

The Energetic Gamma Ray Experiment Telescope (EGRET) on the Compton Gamma Ray Observatory (CGRO) discovered gamma-ray emission from more than 67 blazars during its nine-year lifetime. We conducted an exhaustive search of the EGRET archives and selected all the blazars that were observed multiple times and were bright enough to enable a spectral analysis using standard power-law models. The sample consists of 18 flat-spectrum radio quasars (FSRQs), 6 low-frequency peaked BL Lac objects (LBLs) and 2 high-frequency peaked BL Lac objects (HBLs). We do not detect any clear pattern in the variation of spectral index with flux. Some of the blazars do not show any statistical evidence for spectral variability. The spectrum hardens with increasing flux in a few cases. There is also evidence for a flux-hardness anticorrelation at low fluxes in five blazars. The well observed blazars (3C 279, 3C 273, PKS 0528+134, PKS 1622-297, PKS 0208-512) do not show any overall trend in the long-term spectral dependence on flux, but the sample shows a mixture of hard and soft states. We observed a previously unreported spectral hysteresis at weekly timescales in all three FSRQs for which data from flares lasting for $\sim(3-4)$ weeks were available. All three sources show a counterclockwise rotation despite the widely different flux profiles. We analyze the observed spectral behavior in the context of various inverse Compton mechanisms believed to be responsible for emission in the EGRET energy range. Our analysis uses the EGRET sky maps that were regenerated to include the changes in performance during the mission.

Subject headings: galaxies: active—methods: data analysis, statistical—radiation mechanisms:non-thermal

1. INTRODUCTION

Blazars are a class of active galactic nuclei (AGNs) characterized by highly luminous and rapidly variable continuum emission at all observed frequencies from radio to gamma-rays. Very long baseline interferometry (VLBI) structures of these sources reveal compact cores with jet-like features which often show evidence of superluminal motion (Vermulen & Cohen 1994). The broadband spectral energy distribution (SED) of these sources shows two peaks. It has been widely accepted, in the scenario of leptonic models, that the lower-frequency peak is due to synchrotron emission from relativistic plasma moving along the jet away from the core of the AGN while the second peak is attributed to inverse-Compton scattering of relativistic electrons by soft ambient photons, produced either internal or external to the jet. These “seed-photons” for inverse-Compton emission could come from synchrotron emission itself as postulated by synchrotron-self Compton (SSC) models (Ghisellini et al. 1985; Maraschi, Ghisellini & Celotti 1992; Marscher & Gear 1985; Bloom & Marsher 1996), or they could be en-

tering the jet directly from the accretion disk as in the ECD (external Compton scattering of direct disk radiation) models (Dermer, Schlickeiser & Mastichiadis 1992; Dermer & Schlickeiser 1993), or they could reach the jet after being re-scattered by surrounding broad-line-region (BLR) clouds as in the ECC (external Compton scattering from clouds) models (Sikora, Begelman & Rees 1994; Blandford & Levinson 1995; Dermer, Sturmer & Schlickeiser 1997). In addition, the BLR could also reflect the synchrotron photons back into the jet to undergo inverse-Compton scattering (external-reflection-Compton model; Ghisellini & Madau (1996)). Finally, the seed photons could be produced by the infrared (IR) dust that surrounds the blazar nucleus (external Compton from infrared dust-ERC(IR); Sikora et al. (2002); Blazejowski et al. (2000)). The dust is more concentrated in a torus that lies in the equatorial plane of the blazar (Wagner et al. 1995). Quite often, a combination of these models is required to fit the broadband spectrum of a blazar through the entire range of frequencies from radio to gamma-rays.

Observationally, the class of blazars includes flat-spectrum radio quasars (FSRQs) and BL Lac objects. FSRQs have strong and broad optical emission lines while the lines are weak in BL Lac objects. The position of the peaks in a broadband SED allows a further division of BL Lac objects into two categories: low-frequency-peaked BL Lacs (LBLs) and high-frequency peaked BL Lacs (HBLs). The first peak is at infrared/optical frequencies for *red blazars* which could be either the FSRQs or the Low-frequency-peaked blazars

¹ Department of Physics, University of Maryland at College Park, College Park, MD 20742; giridhar@milkyway.gsfc.nasa.gov

² Exploration of the Universe Division, NASA Goddard Space Flight Center, Greenbelt, MD, 20771

³ Department of Physics and Astronomy, Barnard College and Columbia University, New York, NY 10027

⁴ Space Astronomy and Instrumentation Division, ISRO Satellite Centre, Bangalore, Karnataka, 560017, India

⁵ Astrophysical Institute, Department of Physics and Astronomy, Ohio University, Athens, OH 45701

(LBLs) and at UV/X-rays for *blue blazars* or the High-frequency-peaked blazars (HBLs). The second peak is in the gamma-ray range (MeV-GeV) for LBLs & FSRQs and in the TeV range for HBLs. HBLs are much lower in overall luminosity than FSRQs with LBLs somewhere between (Fossati et al. 1998).

During its nine year lifetime, EGRET has detected GeV-range emission from more than 67 blazars and a number of them have been observed multiple times (Hartman et al. 1999; hereafter 3EG). The EGRET energy range (30 MeV-10 GeV) lies near the maximum or on the falling portion of the inverse-Compton peak for FSRQs and on the rising portion of the peak in the case of HBLs and it lies somewhere in between for LBLs. A continuity in the observed spectral properties of BL Lacs and FSRQs has been postulated by Fossati et al. (1998) with the gamma-ray spectral index getting progressively harder from FSRQs to HBLs. While this trend is expected of the average spectral properties of these sources, previous studies have suggested a hardening of the gamma-ray spectral index in FSRQs with an increase in flux. This was reported for individual blazars in Mukherjee et al. (1995); Sreekumar et al. (1996); Bloom et al. (1997); Stacy et al. (2003) and was also observed in the combined data from 18 brightest blazars (Sreekumar et al. 2001). This feature, coupled with the fact that the average spectral index of 2.15 ± 0.04 measured for blazars (Mukherjee et al. 1997) is quite close to the spectral index of 2.10 ± 0.03 (Sreekumar et al. 1998) for diffuse gamma-ray background, is used to attribute the extragalactic gamma-ray background to emission from unresolved blazars (Stecker & Salamon 1996).

With the EGRET's calibration finalized and its archive now complete, the behavior of gamma-ray spectral index can be studied in detail across different epochs and over a broad range of flux. This paper presents the results of such an effort and is organized as follows. We reanalyzed the entire blazar data from the EGRET mission for this project. Section 2 describes the data and §3 discusses the analysis procedure. We examine the spectral properties of different source classes, the long term and the short term spectral variability in §4, discuss the implications of the results in §5, and summarize in §6.

2. SOURCE SELECTION AND OBSERVATIONS

CGRO was launched on April 5 1991 and it re-entered the earth's atmosphere on June 4, 2000. One of the four instruments on board was EGRET that was sensitive in the energy range 30 MeV-10 GeV. The 3EG contains the basic results (flux and spectral indices) from analysis of all observations until the end of Cycle 4 (1995 October 3). Mukherjee et al. (1997) presented summary results for all blazars detected through the end of Cycle 4 and included the spectral indices for blazars that were detected at a significance greater than 6σ . Although there were very few new detections after Cycle 4 (e.g. PKS 2255-282 and Mrk 501), eight blazars were observed multiple times in Cycles 5-9. Spectral analysis results after Cycle 4 are available only for PKS 0528+134 (Mukherjee et al. 1999), which contains results through the end of Cycle 6.

EGRET viewing periods (VPs) ranged in duration from 3 to 20 days but they were usually a week long. Sometimes an object was observed during two or more

contiguous viewing periods, either as a part of the observing schedule or because the object was in an extremely active state. EGRET was operated with a narrow field of view for most of the latter half of the mission (Cycle 5 onward) to conserve gas lifetime, thus limiting the number of accessible targets. The details (viewing period number, start and end dates) of the viewing periods (after Cycle 4) are listed in columns 1-3 of Table 1. Columns 4 & 5, respectively, list the sources that were in the field of view (FOV) during that time, and their off-axis viewing angle. Information for viewing periods prior to Cycle 5 is listed in 3EG.

We have analyzed all nine years of data for all the blazars seen by EGRET, and these objects are listed in Table 2. The sample consists of 98 sources, 67 of which are confirmed identifications. The 31 "possible" identifications are marked by a question mark in column 2, and the more common names of the sources are listed in column 3. The distribution consists of 66 flat-spectrum radio quasars (FSRQ), 17 LBLs, 4 HBLs, 10 flat-spectrum radio sources (FSRS) and 1 radio galaxy. The classifications (listed in column 10 of Table 2) have been adopted from 3EG and Ghisellini et al. (1998). The 66 flat-spectrum radio quasars have been further classified into 19 high-polarization quasars (FSRQ(HP)), 15 low-polarization quasars (FSRQ(LP)). Polarization information could not be obtained for the remaining. Twenty-six of the 97 sources were observed multiple times and were bright enough during those observations to yield a spectral index. These sources are marked by a "Y" in column 9.

3. ANALYSIS

EGRET was a spark chamber telescope with an effective area of 1000 cm^2 at 150 MeV, 1500 cm^2 between 500 MeV-1 GeV, which decreased gradually to about 700 cm^2 at 10 GeV. The off-axis sensitivity decreased as an approximate Gaussian with a FWHM of $\sim 20^\circ$. The sensitivity beyond 30° was less than 15% of the on-axis sensitivity. Details of the instrument and calibration can be found in Kanbach et al. (1988); Hughes et al. (1980); Thompson et al. (1993); and Esposito et al. (1999). During its nine year lifetime, the spark chamber gas was refilled multiple times (Bertsch et al. 2001), and for most of the latter half of the mission (Cycle 5 onward), EGRET was operated with a narrow FOV (18° useful radius) to conserve gas lifetime. The detection efficiency of EGRET varied throughout the mission due to aging of the spark-chamber gas between refills and a hardware failure in 1997. An energy dependent effect was also observed in the degradation. The method used to calibrate the efficiency up to Cycle 4 (Esposito et al. 1999) did not deal with this energy-dependence adequately. The results in this paper are derived from EGRET maps produced using the calibration described in Bertsch et al. (2001).

One of the standard EGRET data products for any viewing period is a pair of maps showing gamma-ray arrival directions from the observed sky-region in the energy intervals 30-100 MeV and >100 MeV. For the work presented here, these maps were used in conjunction with a list of all the known EGRET-sources, to determine simultaneously the counts from all sources in the field of view and their significance of detection in the two energy-

intervals through a method of maximum likelihood. Details of the maximum likelihood method and the process of determination of the significance of detection can be found in Mattox et al. (1996) and Esposito et al. (1999). All sources that were detected at a significance $< 2\sigma$ in the energy interval >100 MeV were eliminated from the list and the process was repeated again to determine the counts and fluxes (along with the associated errors) for the remaining sources.

If the source of interest was detected at a significance $> 4\sigma$ in the energy interval >100 MeV, then a four point spectrum was determined using counts recorded in the energy intervals (in MeV) 30-100, 100-300, 300-1000 and 1000-10000. The points were fitted with a single power law of the form $F(E) = k(E/E_o)^{-\alpha}$ photons $\text{cm}^{-2} \text{s}^{-1} \text{MeV}^{-1}$ where $F(E)$ is the flux, α the photon spectral index, E the photon energy, E_o the energy normalization factor and k a coefficient of normalization.

If the overall significance of detection of the source was greater than 6σ , the energy intervals with a strong detection were further split up into smaller intervals (for which standard EGRET maps exist) to determine the spectral index. For the strongest sources, the standard 10 intervals 30-50, 50-70, 70-100, 100-150, 150-300, 300-500, 500-1000, 1000-2000, 2000-4000, 4000-10000 (all in MeV) were utilized. Most of the spectra after Cycle 5 had to be determined using 4-5 energy intervals (when a source was not undergoing a flare). Figure 1 shows sample four-point spectra from PKS 1622-297 and a 5-point spectrum from 3C 279. Analysis using the new maps has constrained the spectral indices better (lower errors) for a majority of the sources. Previous EGRET spectral analyses required a minimum of 6-sigma significance of source detection and used 10 energy bins to calculate the spectrum. We have used a slightly different approach, lowering the cutoff to 4 sigma. This does not affect the quality of the spectral analysis since we are using only 4-5 energy intervals for computing the spectral indices for faint sources, giving us better statistics in each bin, and lowering the errors. In addition, we found that the spectral index was within the error bars of the index calculated using 10 energy bins.

Some of the blazars considered here were part of extended campaigns. If the source was not very bright during such times, adjacent viewing periods were combined. The analysis process was then repeated with the combined data, and an attempt was made to extract the spectrum. The longest period for which a source was in EGRET's field of view continuously was 49 days (7 viewing periods), for 3C 273 and 3C 279. Sometimes, all the observations during a cycle had to be combined to obtain a reliable detection and spectrum.

We have done a complete spectral analysis for all the blazars detected by EGRET using the recalibrated data products. Table 2 (column 6) shows their average photon spectral indices. For the bright blazars that were observed multiple times, we used the sample mean and standard deviation (of mean) as the spectral index. For the rest, we used the spectral index from all the data available unless a source was bright during one of the observations and was almost inactive during the rest of the viewing periods. Column 7 lists the mean flux (> 100 MeV) recorded for these sources in units of 10^{-8} photons

$\text{cm}^{-2} \text{sec}^{-1}$. Table 3 lists the results of spectral analyses for sources which yielded more than one spectral index value. Columns 5, 6 & 7 list the spectral index, flux and the detection significance, respectively. The viewing periods that were combined to get the spectra are listed in column 3 while their corresponding starting dates are listed in column 2 in the same order. For identification purposes, each of these observations is labeled in the spectral index vs. flux plot shown in Figure 3, with the labels listed in column 4 of Table 3.

4. RESULTS

4.1. Gamma-ray spectral distribution

Since a classification of blazars was based on the location of the synchrotron peak, we searched the literature for multiwavelength fits to data from all the blazars detected by EGRET, in order to determine the frequency of their synchrotron peaks and to examine its dependence on the gamma-ray spectral index. Multiwavelength fits to the broadband spectrum ($\log(\nu F_\nu)$ vs $\log(\nu)$) from simultaneous data are available for more than one epoch for: 3C 279 (Hartman et al. 2001; Ballo et al. 2002), BL Lac (Böttcher & Bloom 2000), 3C 273 (Kataoka et al. 2002), PKS 2155-304 (Chiappetti et al. 1999; Kataoka et al. 2000), Mrk 421 (Takahashi et al. 2000; Krawczynski et al. 2001), Mrk 501 (Tavecchio et al. 2001; Kataoka et al. 1999; Krawczynski et al. 2002; Petry et al. 2000), PKS 0528+134 (Mukherjee et al. 1999). For the rest of the blazars, we used values from Ghisellini et al. (1998) & von Montigny et al. (1995) that are compilations of multiwavelength data (simultaneous and non-simultaneous) from literature and corresponding broadband model-fits. In cases where there is more than one fit available, or when a clear determination of the peak was not possible, the peak frequency was fixed at the average value and the error was calculated from one of the extremes. The logarithm of synchrotron peak frequency values have been listed in column 8 of Table 2.

The plot of gamma ray spectral index vs log synchrotron peak frequency for the blazars in our sample is shown in Figure 2. The sample of sources shown in the plot consists of 37 FSRQs, 10 LBLs and 3 HBLs. The blazars for which we could not find the synchrotron peak frequency in the literature have been excluded from the figure. Since FSRQs have the lowest synchrotron-peak frequency and the EGRET energy range lies on the decreasing portion of their inverse Compton peak (in a plot of the broadband spectral energy distribution), they are expected to have soft spectral indices. HBLs have the highest synchrotron peak frequency and the EGRET-range lies on the rising portion of their inverse Compton peak. Consequently, they are expected to have hard spectral indices. LBLs lie somewhere in between. Under this unified-blazar paradigm, a plot of gamma-ray spectral indices vs. synchrotron peak frequencies should have a smooth variation from FSRQs to LBLs to HBLs (Fossati et al. 1998). A plot similar to that shown in Figure 2 was made in the past for 27 blazars using data through Cycle 4 (Lin et al. 1999). A comparison of our data with this work shows that some of the spectral indices obtained by us are different, due to the availability

of more data and the recalibration of the raw data products, as described earlier (see section 3).

We obtained a mean spectral index of 2.26 ± 0.03 for the 66 FSRQs, 2.14 ± 0.08 for the 17 LBLs, 1.68 ± 0.09 for the 3 HBLs and 2.48 ± 0.1 for the 10 other flat spectrum radio sources (FSRS). The spectral index for FSRQs with high polarization (HP) and low polarization (LP) was 2.19 ± 0.06 and 2.32 ± 0.06 respectively. The spectral index increases across HBLs, LBLs, FSRQs(HP) and FSRQs(LP). This is consistent with the prediction that the spectral properties of blazars form a well defined sequence from HBLs to LBLs to FSRQs (HP,LP) (Ghisellini et al. 1998; Fossati et al. 1998).

4.2. Spectral variability with Flux

4.2.1. Long term spectral variability

We searched for variability in the spectral index of all the blazars (for which two or more spectral indices could be calculated) using the χ^2 test and the results are listed in Table 4. Column 2 contains the sample mean (Γ_μ) and the standard deviation of the mean (σ) for each blazar. The χ_{red}^2 value obtained from fitting the sample of spectral indices with a line of constant mean Γ_μ is listed in column 3. Column 4 lists the degrees of freedom (DOF) (which is one less than the sample size), while column 5 contains the confidence level for the presence of spectral variability. We do not detect any statistical evidence for spectral variability in 16 of the 26 blazars. The confidence levels for the presence of spectral variability are low ($< 80\%$), mostly due to the large error bars on the spectral indices.

We looked for spectral variability correlated with flux using the Pearson's correlation coefficient. The correlation coefficient is listed in column 6 of Table 4. The coefficient, which could be calculated only in cases where there were three or more observations, is negative when the spectral index (positive) hardens with increasing flux. The dependence of spectral index on flux is not uniform across all the blazars. The index hardens with increasing flux in some cases, softens in others, and in the rest does not vary with flux. Using a cutoff of 0.8 for the correlation coefficient, we found the spectral index to be correlated with flux in 10 of the 26 blazars (including those with two observations where there was visual evidence). The spectrum hardened with increasing flux in 6 of them while the spectrum softened in the remaining 4. Only five sources satisfied both the spectral variability and the index-flux correlation criteria: PKS 0537-441, 1222+216 (4C 21.35), PKS 1633+382 (4C+38.41), 2200+420 (BL Lac) and 2230+114. We discuss some individual sources below.

1253-055 (3C 279): This object shows spectral variability at a confidence level of 99.99% and shows marginal evidence for hardening with increase in flux. The spectral states at a flux $> 70 \times 10^{-8}$ photons $\text{cm}^{-2} \text{s}^{-1}$ span more than 85% of the range of fluxes observed. These states do not show any overall trend in the spectral index vs. flux space (correlation coefficient of 0.05) and do not show any significant evidence for spectral variability (confidence level of 58%). The quiescent states from Cycles 3 and 4 have a softer spectral index when compared with the average value of 1.96 while the quiescent state from Cycle 6 has a harder spectral index.

PKS 0208-512: We do not see any overall trend for this source, in spite of a strong evidence for spectral variability (confidence of 98%). However, the spectral index does show evidence of hardening with increasing flux (correlation coefficient of -0.95) at fluxes higher than 60×10^{-8} photons $\text{cm}^{-2} \text{s}^{-1}$. A similar trend was also observed in this source by Stacy et al. (2003) who combined simultaneous data from the Compton Telescope (COMPTEL; 0.75-30 MeV) and EGRET. They obtained a correlation coefficient of -0.78 between the spectral index in the 0.75 MeV - 10 GeV range and the flux (> 100 MeV) recorded in the EGRET energy range.

We observe a softening in the spectral index (coefficient of +0.95) as the flux increases, at fluxes lower than 80×10^{-8} units. There is an indication of this effect at lower fluxes in Stacy et al. (2003, see their Figure 4), but the large error bars do not justify a separate fit. Moreover, PKS 0208-512 has been categorized as an "MeV-blazar" and the spectrum from these sources shows a break between 1-20 MeV (Sikora et al. 2002; Skibo et al. 1997; Blom et al. 1995; Collmar et al. 1997). Hence, a single power law does not adequately describe the entire energy range from 0.75 MeV-10 GeV. Flux anti-correlations between COMPTEL and EGRET could also be expected for MeV-blazars (observed in case of PKS 0528+134, also a possible MeV blazar; Collmar et al. (1997)). But a reanalysis of the 1993 COMPTEL data by Stacy et al. (2003) lowered the significance of the only detection of this source in the MeV energy range, with no detections in its many subsequent observations. Consequently, the association of PKS 0208-512 with MeV-blazars is questionable. But the unique nature of the spectral dependence on flux (initial softening and subsequent hardening) in the EGRET energy range, makes this strong gamma-ray source an interesting candidate for future observations.

PKS 0528+134: Previously published results for this object (Mukherjee et al. 1996) showed a correlation of -0.85 between spectral index and flux using data from viewing periods 0.2-0.5 (combined), 1.0, and 213.0. The same combination of viewing periods using recalibrated data did not show any evidence of spectral hardening. Inclusion of data through viewing period 420.0 decreased the correlation to -0.5 (Mukherjee et al. 1999). We obtained a correlation coefficient -0.5 for the complete data which included observations from Cycles 5 and 6. The large error bars yield a low confidence of spectral variability of 67% despite a spread in the values.

PKS 0537-441, PKS 1633+382 (4C+38.41): Spectral indices for these objects harden with increasing flux (correlation coefficients of -0.97 & 0.99) and show spectral variability at a confidence of 87% and 98% respectively.

2200+420 (BL Lac) & 2230+114 (CTA 102): The spectrum hardens with increasing flux in these sources. The correlation coefficient was not calculated in these cases as there were only two observations.

Some of the FSRQs and LBLs show spectra that appear to soften with increasing flux. This can be seen in PKS 1222+216 (4C 21.35), PKS 1219+285 (ON 231), and, also in PKS 0208-512 and S5 0716+714 at low fluxes.

HBLs; 1101+384 (Mrk 421) & PKS 2155-304: The

spectral index for Mrk 421 hardens as flux increases with a coefficient of -0.997. PKS 2155-304, however, shows a softening in spectral index with increasing flux (correlation coefficient of +0.99). This seems to be in contradiction to standard scenario wherein the gamma-ray emission from HBLs is from SSC mechanism (Böttcher & Chiang 2002; Li & Kusunose 2000). HBLs are not very bright at EGRET energies and some of the spectral states show deviations from a simple power-law fit. Consequently, the error bars on the spectral indices are large and the confidence level of spectral variability from the χ^2 test is low.

4.2.2. Short term spectral variability: Spectral hysteresis during a flare

Blazars vary on multiple timescales. The smallest timescale of resolution (based on the light curves) for a gamma-ray flares is about $\sim 3 - 8$ hours (Mattox et al. 1997; Nandikotkur 1997). A study of spectral hysteresis (in relation to flux) during flares provides crucial insights into factors related to the comoving electron dynamics (electron acceleration and cooling) (Kusunose, Takahara & Li 2000; Li & Kusunose 2000; Böttcher & Chiang 2002). Since we have extracted spectral indices from data accumulated over a complete viewing period (usually 7 days long), we cannot track spectral changes during a flare. Some of the sources, however, were observed for more than 2 consecutive viewing periods when they were flaring, either because the observations were planned a priori, or because the schedule was changed to track the flare. The flux history in such cases could show an event occurring at larger timescales. Figure 4 shows the light curve and spectral index vs. flux plots of the flare for the three sources for which we had data from four contiguous viewing periods. We discuss the individual sources below.

PKS 1622-297: This source was observed from June 6, 1995 (VP 421.0) until July 7, 1995 (VP 423.5) for 4 consecutive viewing periods when it underwent a large flare. Mattox et al. (1997) split the observations into 10 unequal intervals with the size of the intervals ranging from 1 day to 10 days. A plot between flux in the two intervals- 100 MeV-300 MeV (x) and > 300 MeV (y) showed a clockwise progression in time. Previously published spectral index values (Mukherjee et al. 1997) for the four viewing periods during this flare show evidence for spectral variability at a confidence level of 97% (χ^2 of 9.81 with 3 degrees of freedom) but a large fraction (68%) of χ^2 was due to the hard spectral index of 1.72 ± 0.15 during viewing period 422.0, which recorded the largest flux. We obtained a spectral index of 2.22 ± 0.11 for this viewing period with the recalibrated maps. A χ^2 test yielded confidence level of 51%, with most of the contribution from viewing period 421.0. The spectral indices trace out a counterclockwise loop (as time progresses) in the spectral index-flux space.

PKS 1406-076: Four out of the five points for this object are from 4 consecutive viewing periods from December 22, 1992 (VP 204.0) till February 2, 1993 (VP 207.0). While the light curve shows two successive flares, the large error bars on the spectral indices reduce the variability in spectral index to a confidence of 62%. The spectral indices show a counterclockwise progression during the period.

PKS 0528+134: Observations of this object in April-May 1991 spanned 36 days. The source was observed from April 4, 1991 to May 4, 1991 and then for 2 weeks from May 16, 1991, and a week from June 6, 1991. These points are marked with their viewing-periods number (0.2-0.5, 1.0 & 2.1) in Figure 3. The χ^2 test shows spectral variability at a confidence level of 73%, which is the largest among the three sources. The light curve in Figure 4 shows the contiguous viewing periods 0.2-0.5 to be a part of a single event and the spectral index traces out an intertwined loop in counterclockwise direction as in the other cases.

Spectral hysteresis is a commonly observed phenomenon in HBLs at X-ray wavelengths. It has been reported at multiple timescales ranging from hours (Takahashi et al. 1996; Sembay et al. 1993; Gliozzi et al. 2006) to seconds (Cui 2004) indicating the presence of scale invariance in the spectral evolution at X-ray wavelengths. We have observed hysteresis at weekly timescales in all the three FSRQs for which data from at least 4 contiguous viewing periods was available. This effect has previously never been observed in FSRQs in gamma-rays at these timescales. The light curve in Figure 4 shows completely different flare profiles for the 3 blazars. The flare in PKS 0528+134 is a combination of a slow rising phase accompanied by a faster decaying phase while the profile in PKS 1622-297 is exactly the opposite with a fast rise and a comparatively slower decay. The light curve in the case of PKS 1406-076 shows multiple events- a flare consisting of a uniform rise and decay, and a second flare that was partially captured. Although the flux profiles are quite different, all the three sources show a counterclockwise rotation in the spectral index vs. flux space as time progresses.

5. DISCUSSION

Under a leptonic jet paradigm, the broadband spectral energy distribution of blazars is modeled by considering synchrotron and inverse Compton emission from a blob of e^+e^- plasma moving relativistically along the jet axis. The seed photons for the inverse Compton process could come from the jet (SSC), the accretion disk (ECD), the broad line region clouds (ECC) or the infra-red dust in the surrounding torus ERC(IR) (see §1 for the references for various emission mechanisms).

5.1. Spectral variability in FSRQs and LBLs

External-Compton process appears to play an important role in FSRQs and LBLs (Ghisellini et al. 1998). In a broadband spectral energy distribution, the peak emission frequency for ERC(IR), ECD and ECC processes increases in that order. The latter two have their peak frequency in the EGRET energy range and affect spectral variations in a more direct way. However, not all FSRQs have a strong infra-red component since it depends on the size of the torus and the density of the circum-nuclear dust. The inverse Compton component due to SSC emission does not have a pronounced peak. The plateau of the SSC emission extends from hard X-rays (few hundred keV) to the GeV gamma-ray region.

When the source is in a low-intermediate state, emission from the SSC process is at least as important as that from the three ERC processes, and the photon

spectrum could be hard or soft, based on relative fraction of flux from these processes. Model fits to the broadband spectrum from 3C 279 by Hartman et al. (2001) & Ballo et al. (2002) and PKS 0528+134 by Mukherjee et al. (1999) show that moderate-large flares require a greater contribution from the ERC processes and have a higher bulk Lorentz factor Γ for the particles.

As the source undergoes a flare, the energy density of the IR field and the broad line field (BEL), both of which are proportional to Γ^2 (Sikora et al. 2002) as measured in the comoving frame of the plasma, also increase. The flares might also be related to the injection of energetic particles near the base of the jet, where the external radiation fields have a higher density than further out. Consequently, the contribution of external Compton processes increases. Although emission from all processes increases, the ECD and ECC processes affect the EGRET energy range more. However, the extent of contribution from the ERC(IR) process, whose peak lies below the EGRET energy range (Blazejowski et al. 2000), could be one of the factors that determines how soft the EGRET spectrum is during the low-intermediate states as it affects the lower energies of the EGRET range. Broadband fits for 3C 279 from various epochs in Hartman et al. (2001, their fig. 2) show the low-intermediate states (Cycle 3, 4 & 6 in our Figure 3) to have comparable fluxes from SSC, ECD, and ECC processes, with the EGRET data lying on the falling portion of the SSC emission plateau. The 0.3-30 MeV region, which is just below EGRET energy-range, shows a significant excess (in the broadband fits for Cycles 3 and 4) that could be caused by the ERC(IR) process (not included in the model). Hence the resultant EGRET spectra are soft. The enhanced MeV emission could also explain the softening in the spectral index seen from low to intermediate fluxes in PKS 0208-512, which has been categorized as an ‘‘MeV-blazar’’ (Skibo et al. 1997; Blom et al. 1995) and more recently questioned by Stacy et al. (2003). The existence of MeV-blazars as a separate class has been disputed due to the dearth of sources. However the Swift Burst Alert Telescope has recently detected bright emission, and rapid variability at short timescales (down to 1-2 ks) from the optically faint quasar J0746 in the 15-195 keV range leading to the inclusion of this blazar in the MeV-blazar class (Sambruna et al. 2006).

While the ERC(IR) process could play an important role during the low-intermediate states, there is a substantial increase in emission from the ECD and ECC process during large flares, as shown in the case of 3C 279 by Hartman et al. (2001). The EGRET spectrum during these flares is hard or soft based on the relative contribution from these two processes. Since the IR emitting region is very large and far away, the ERC(IR) process does not vary over timescales as short as those of the other two process and does not play a significant role in the spectral variations seen at short time scales during flares that typically last a few days.

Spectral hysteresis: The three sources (PKS 1622-297, PKS 0528+134, PKS 1406-076) that were observed for an extended time during flares, show evidence of counterclockwise spectral hysteresis. A possible explanation for this may be the emergence of an external Compton component near the onset of the flare, where an ERC

component at MeV-GeV energies might be dominant. As the flare evolves and the emission region moves out, the intrinsically harder SSC radiation might take over (as it takes time $\sim R/c$ for the internal radiation field to build up), leading to hardening of the spectrum as the flux is already decreasing. This would work in situations in which the acceleration time scale is shorter than the cooling time scale, and the cooling time scale is of the order of the dynamical time scale, R/c .

5.2. Spectral variability in HBLs- a possible external component?

Inverse Compton emission in the case of HBLs is usually attributed to the SSC mechanism. The EGRET energy range lies on the rising portion the inverse Compton bump for Mrk 421. As the source undergoes a flare, the maximum flux at the peak increases, leading to increased contribution at higher frequencies on the low energy tail of the inverse Compton bump causing the spectra to harden. In PKS 2155-304, however, we observed the opposite trend of spectrum softening with increasing flux. This is in contradiction with the standard SSC interpretation (Kusunose, Takahara & Li 2000; Li & Kusunose 2000; Böttcher & Chiang 2002). The soft spectral index (2.22 ± 0.46) is from the flare in November 1997 (viewing period 701.0 in Figure 3). In a broadband distribution (plot of νF_ν vs ν), a photon spectral index of 2 is a horizontal line. The rising portion of inverse-Compton peak has a spectral index less than 2 while the decreasing portion of the synchrotron peak would have a photon spectral index of greater than 2. If the frequency range of observations is close to the frequency where these two branches meet, it is possible for the synchrotron branch to move in to the observed energy range during flares leading to a spectral index that is higher than 2.0. But the EGRET energy range is quite far from where the two branches meet in case of PKS 2155-304 (Kataoka et al. 2000, see their fig. 7). Extending the synchrotron emission up to EGRET energies would come close to the theoretical limit for synchrotron emission from leptons for Doppler factors usually seen in such sources. The observed trend in PKS 2155-304 could be an indication for a quasi- external Compton component expected from a decelerating-jet model (Georganopoulos & Kazanas 2003), where synchrotron emission from a previous, slower component may provide an additional target photon field for Compton scattering. Alternatively, this could be a signature of proton synchrotron emission in a hybrid leptonic/hadronic model (Mücke et al. 2003) since one would expect that there might be a non-negligible proton fraction present in the jet.

While the varying dominance of ERC components (or an absence thereof) can explain some of the gamma-ray spectral variability observed so far, it is just one of the many possible scenarios. Gamma-ray spectral variability could arise out of a combination of factors that are both internal and external to the plasma. The internal factors affect the two energy cutoffs of the particle injection spectrum, the injection spectral index, the injection energy, the magnetic field, the bulk Lorentz factor of plasma and the particle density. The external factors are: the energy density of the infra-red field due to the dusty torus, the energy density of the broad emission line region, and the

level of accretion disk activity. The current gamma-ray data, however, do not allow us to effectively explore the large parameter space as the error bars on the spectral indices are usually high. This is due to the limitations of EGRET's sensitivity. The Gamma-ray Large Area Space telescope (GLAST)⁶ with a higher sensitivity and greater duty cycle of coverage for individual sources should be able to determine spectral indices more accurately. In addition to the large number of parameters that go into the jet models, the long integration times of EGRET imply that we are averaging over substantial and completely arbitrary sections of individual outbursts, or adding contributions from multiple smaller outbursts. A study of spectral hysteresis during individual flares could indicate if we are dealing with global, structural changes (including, e.g., a change of the bulk Lorentz factor), or with factors related to the co-moving electron dynamics (electron acceleration/cooling) (Kusunose, Takahara & Li 2000; Li & Kusunose 2000; Böttcher & Chiang 2002). The EGRET data do not allow us to study spectral evolution during a flare. This would be an area of study ideal for GLAST.

5.3. Blazars as a source of extragalactic gamma-ray background

Stecker & Salamon (1996) postulated that the *entire* diffuse extragalactic gamma-ray background (EGRB) can be attributed to emission from unresolved blazars, based on two factors: (1) The spectral index for diffuse gamma-ray background is 2.10 ± 0.03 (Sreekumar et al. 1998), which is quite close to the previously published value of the average spectral index (2.15 ± 0.04) for all observed blazars (Mukherjee et al. 1997) and (2) The preliminary concave shape of the extragalactic gamma-ray background, determined prior to 1995, could be well fitted by the diffuse emission calculated from the blazar luminosity function (Stecker & Salamon 1996, their Figure 3). However, the EGRB spectrum published in Sreekumar et al. (1998) shows deviations from a power-law index of 2.1 ± 0.03 at low and high energies. The curvature is less prominent but it cannot be ruled out. In addition, the flare-state spectra had to be harder than the quiescent state spectra for a good fit (Stecker & Salamon 1996, their Figure 3).

We obtained a value of 2.25 ± 0.03 (2.22 ± 0.03 for FSRQ+LBL+HBL) for the average spectral index of all the blazars observed by EGRET and a median value of 2.25. 64 of the blazars have spectral indices ≥ 2.1 while 33 of them have spectral indices that were lower.

A more current background spectrum generated using the finalized EGRET data from Cycles 1-4, based on a model different than that used in Sreekumar et al. (1998), was published by Strong et al. (2004) and is shown in Figure 5. The broadband spectrum from 30 MeV -50 GeV shows a clear break at 2 GeV. The spectrum is steeper than the spectrum in Sreekumar et al. (1998) at energies below 2 GeV. The spectrum has a concave curvature due to the break and the rise beyond 10 GeV. Although the whole range from 30 MeV -50 GeV shows substantial deviations from a power law fit, we find that the points below 2 GeV can be fitted well with a power law of slope 2.24 ± 0.01 and a correlation coeffi-

cient of 0.99. The slope is very close to our value for the average blazar spectral index of 2.25 ± 0.03 (superposed in Figure 5).

As we noted earlier, if the EGRB has to be entirely due to blazars, then the flare-state spectra must be harder than the quiescent state spectra to produce concave shape in the diffuse background spectrum (Stecker & Salamon 1996). We did not observe any strong evidence for the flaring states to have a harder spectrum in case of the well-observed blazars. The spectrum hardened with increasing flux in some of them while it softened in some others. For some blazars, both trends were observed. Consequently, any discussion of blazars as sole contributors to diffuse extragalactic background depends on the similarity of the blazar spectrum to that of the EGRB. The proximity of two indices below 2 GeV certainly makes blazars a prime candidate for contributing to the diffuse background.

The current blazar data shows some deviations from power law during flares in some cases, but at energies below 2 GeV. However the data do not have enough statistics to attempt a detailed analysis using broken power law models. Although the blazar spectrum cannot be measured accurately above 2 GeV due to EGRET's limited sensitivity there is no a priori reason to expect a sharp break in the blazar spectrum at 2 GeV along with an increasing contribution at energies higher. This suggests the necessity of an increased contribution by other sources to the extragalactic gamma-ray background at higher energies. The current estimates for blazar contribution to the diffuse background emission range from nearly 100% (Stecker & Salamon 1996) to 25% (Chiang & Mukherjee 1998; Mücke & Pohl 2000). GLAST, with its higher sensitivity and larger energy range (up to 100 GeV) would be able to measure the diffuse background more accurately and help narrow down the class of sources contributing to it.

6. CONCLUSIONS

We analyzed all nine years of EGRET data for blazars and noted the following.

1. The sample contained 98 sources: 66 FSRQs, 17 LBLs, 4 HBLs, 10 FSR sources and 1 radio galaxy. We obtained a mean spectral index of 2.26 ± 0.03 for FSRQs, 2.14 ± 0.08 for LBLs, 1.68 ± 0.09 for HBLs (spectral index could not be calculated for one of them), and 2.48 ± 0.1 for flat spectrum radio sources. The gamma-ray spectral index shows a transition from FSRQs to LBLs to HBLs with FSRQs having the softest spectral index and HBLs having the hardest.
2. We did not observe any clear correlation between the gamma-ray spectral index and flux. A majority of blazars did not show any overall trend. The spectra hardened with increasing flux in some, while it softened in some energy intervals for few others. For those blazars where the spectra varied and did not show an overall trend, the sample consisted of a mixture of hard and soft states.
3. We observed a previously unreported counterclockwise hysteresis at weekly timescales in the spectral index vs. flux space. The effect was consistently

⁶ <http://glast.gsfc.nasa.gov>

seen in the flare data from all the 3 FSRQs which were observed for at least 4 contiguous viewing periods during the flare. The flux profiles of these sources were very different from each other.

4. It is difficult to understand clearly and categorize the observed gamma-ray spectral variability (or a lack thereof) in blazars due to the large error bars on spectral indices and the long integration times needed to get the spectral information.
5. Gamma-ray spectral variability can arise out of a combination of several physical parameters that are both internal and external to the jet. The current data do not have the required energy and time resolution to narrow down the parameter-space used in the models due to EGRET's limitations. GLAST should be able to provide more accurate spectral information on shorter timescales.
6. It is reasonable to expect that there might be deviations from power law behavior in the gamma-ray photon spectrum, given the many possible types of emission mechanisms in blazars. There is some evidence of this in the EGRET data during large flares but insufficient statistics prevent a detailed analysis using broken power law models. This would be an ideal area for GLAST to study.
7. HBLs are faint at EGRET energies. This results in

a low confidence of spectral variability even when there is a strong correlation between spectral index and flux. With the enhanced energy resolution and sensitivity of GLAST, as well as the new atmospheric Cherenkov telescopes (e.g. H.E.S.S., VERITAS, MAGIC and CANGAROO), it should be possible to detect more HBLs at gamma-ray energies and determine their spectral indices more accurately.

8. We obtained a value of 2.25 ± 0.03 for the average spectral index of all the blazars observed by EGRET. This is very close to the spectral index of 2.24 ± 0.01 for the extragalactic gamma-ray background observed below 2 GeV which make blazars as one of the significant contributors to the EGRB. But the break in the broadband background spectrum at 2 GeV and a subsequent increase (>10 GeV) suggests the necessity of an increased contribution by other sources at higher energies.

We would like to thank Olaf Reimer and Andrew Strong for their inputs on the extragalactic gamma ray background and providing us with the data for Figure 5. G.N. would like to thank the Leon Herreid Foundation whose fellowship made a part of this research possible. G.N. would also like to thank Sangeeta Parashar for editing the manuscript.

REFERENCES

- Ballo, L., et al. 2002, ApJ, 567, 50
 Bertsch, D. L., et al. 2001, in Gamma 2001, ed. Ritz, S., Gehrels, N., Shrader, C. R., AIP conference Proceedings, 587
 Blandford, R., & Levinson A. 1995, ApJ, 441, 79
 Blazejowski, M., et al. 2000, ApJ, 545, 107
 Blom, J. J., et al. 1995, A&A, 298, L33
 Bloom, S. D., et al. 1997, ApJ, 490, L145
 Bloom S. D., & Marscher, A. 1996, ApJ, 461, 657
 Böttcher, M., & Bloom, S. D. 2000, AJ, 119, 469
 Böttcher, M., & Chiang, J. 2002, ApJ, 581, 127
 Chiang, J., & Mukherjee, R. 1998, ApJ, 496, 754
 Chiappetti, L., et al. 1999, ApJ, 521, 552
 Collmar, W., et al. 1997, A&A, 328, 33
 Cui, Wei., 2004, ApJ, 605, 662
 Dermer, C.D., Schlickeiser, R., & Mastichiadis, A. 1992, A&A, 256, L27
 Dermer, C.D., & Schlickeiser, R. 1993, ApJ, 416, 458
 Dermer, C.D., Sturmer, S.J., & Schlickeiser, R. 1997, ApJS, 109, 103
 Esposito, J. A., et al. 1999, ApJS, L23, 203
 Fossati, G., et al., 1998, MNRAS, 299, 433
 Georganopoulos, M., & Kazanas, D. 2003, ApJ, 594, L27
 Ghisellini, G., Maraschi, L., & Treves, A. 1985, A&A, 146, 204
 Ghisellini, G., & Madau, P. 1996, MNRAS, 280, 67
 Ghisellini, G., et al. 1998, MNRAS, 301, 451
 Gliozzi, M., et al. 2006, astro-ph/0603693
 Hartman, R. C., et al. 1997, Proceedings of the Fourth Compton Symposium, AIP Conference Proceedings, 410, 307
 Hartman, R. C., et al. 1999, ApJS, 123, 79
 Hartman, R. C., et al. 2001, ApJ, 553, 683
 Hughes, E. B., et al. 1980, IEEE Trans. Nucl. Sci., NS-27, 364
 Kanbach, G., et al. 1988, Space Sci. Rev., 49, 69
 Kataoka, J., et al. 1999, ApJ, 514, 138
 Kataoka, J., et al. 2000, ApJ, 528, 243
 Kataoka, J., et al. 2002, MNRAS, 336, 932
 Krawczynski, H., et al. 2001, ApJ, 559, 187
 Krawczynski, H., Coppi, P., & Aharonian, F.A. 2002, MNRAS, 336, 721
 Kusunose, M., Takahara, F., & Li, H. 2000, ApJ, 536, 299
 Li, H. & Kusunose, M. 2000, ApJ, 536, 729
 Lin, Y. C., et al. 1999, ApJ, 525, 191
 Maraschi, L., Ghisellini, G., & Celotti, A. 1992, ApJ, 397, L5
 Marscher, A.P., & Gear, W.K. 1985, ApJ, 298, 114
 Mattox, J.R. 1996, ApJ, 461, 396
 Mattox, J.R. 1997, ApJ, 476, 692
 Mücke, A., & Pohl, M. 2000, MNRAS, 312, 177
 Mücke, A., et al. 2003, Astropart. Phys., 18, 593
 Mukherjee, R., et al. 1995, ApJ, 445, 189
 Mukherjee, R., et al. 1996, ApJ, 470, 831
 Mukherjee, R., et al. 1997, ApJ, 490, 116
 Mukherjee, R., et al. 1999, ApJ, 527, 132
 Nandikotkur, G., M.S. thesis, Iowa State University, 1997
 Petry, D., et al. 2000, ApJ, 536, 742
 Sambruna et al. 2006, ApJ, 646, 23
 Sembay, S., et al. 1993, ApJ, 404, 112
 Sikora M., Begelman M. C., & Rees, M. J. 1994, ApJ, 421, 153
 Sikora M., et al. 2002, ApJ, 577, 78
 Skibo J. G., Dermer, C.D., & Schlickeiser, R.C. 1997, ApJ, 483, 56
 Sreekumar, P., et al. 1996, ApJ, 464, 628
 Sreekumar, P., et al. 1998, ApJ, 494, 523
 Sreekumar, P., et al. 2001 in in Gamma 2001, ed. Ritz, S., Gehrels, N., Shrader, C. R., AIP conference Proceedings, 587, 314
 Stacy, J. G., Vestrand, W. T., & Sreekumar, P. 2003, ApJ, 598, 216
 Stecker, F. W., & Salamon, M. H. 1996, ApJ, 464, 600
 Strong, A. W., Moskalenko, I. V., & Reimer, O., 2004, ApJ, 613, 956
 Takahashi, T., et al. 1996, ApJ, 470, L89
 Takahashi, T., et al. 2000, ApJ, 542, L105
 Tavecchio, F., et al. 2001, ApJ, 554, 725
 Thompson, D. J., et al. 1993, ApJS, 86, 629
 Vermeulen, R. C., & Cohen, M. H. 1994, ApJ, 430, 467
 von Montigny, C., et al. 1995, ApJ, 440, 525
 Wagner, S. J., et al. 1995, A&A, 298, 688

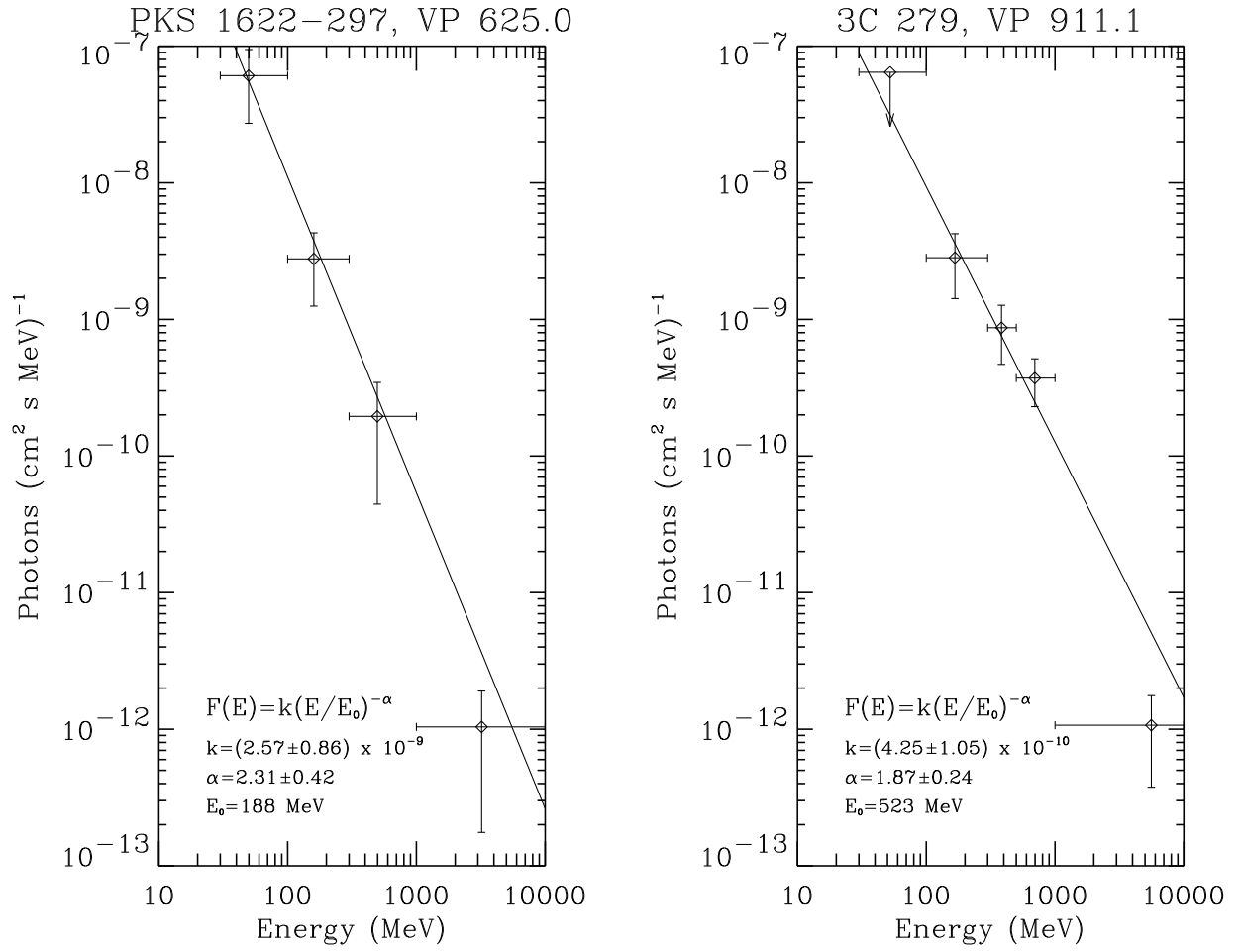


FIG. 1.— Sample EGRET spectra of blazars. Left: PKS 1622-297 in August 1997. Right: 3C 279 during the flare in February 2000. The straight line is a power law fit to the data. The fit parameters (discussed in section 3) are included in the figure.

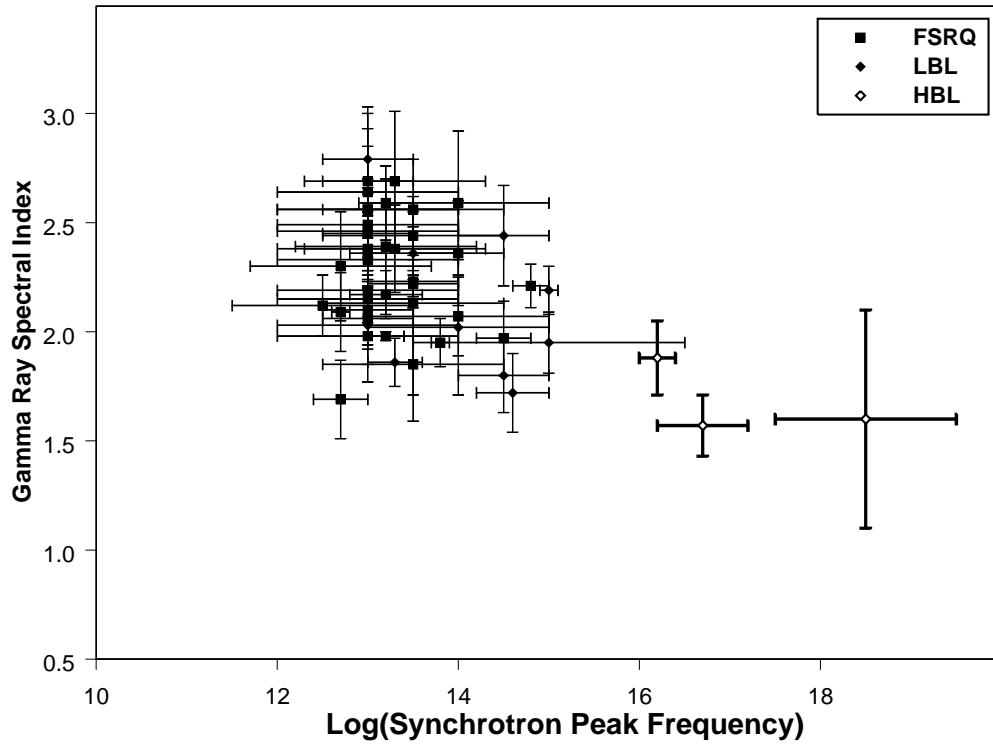


FIG. 2.— Spectral index vs Log(Synchrotron Peak Frequency) of blazars. Classifications are based on Ghisellini et al. (1998) and Hartman et al. (1997). The sample of sources shown in the plot consists of 37 FSRQs, 10 LBLs and 3 HBLs. The data for the plot comes from Table 2

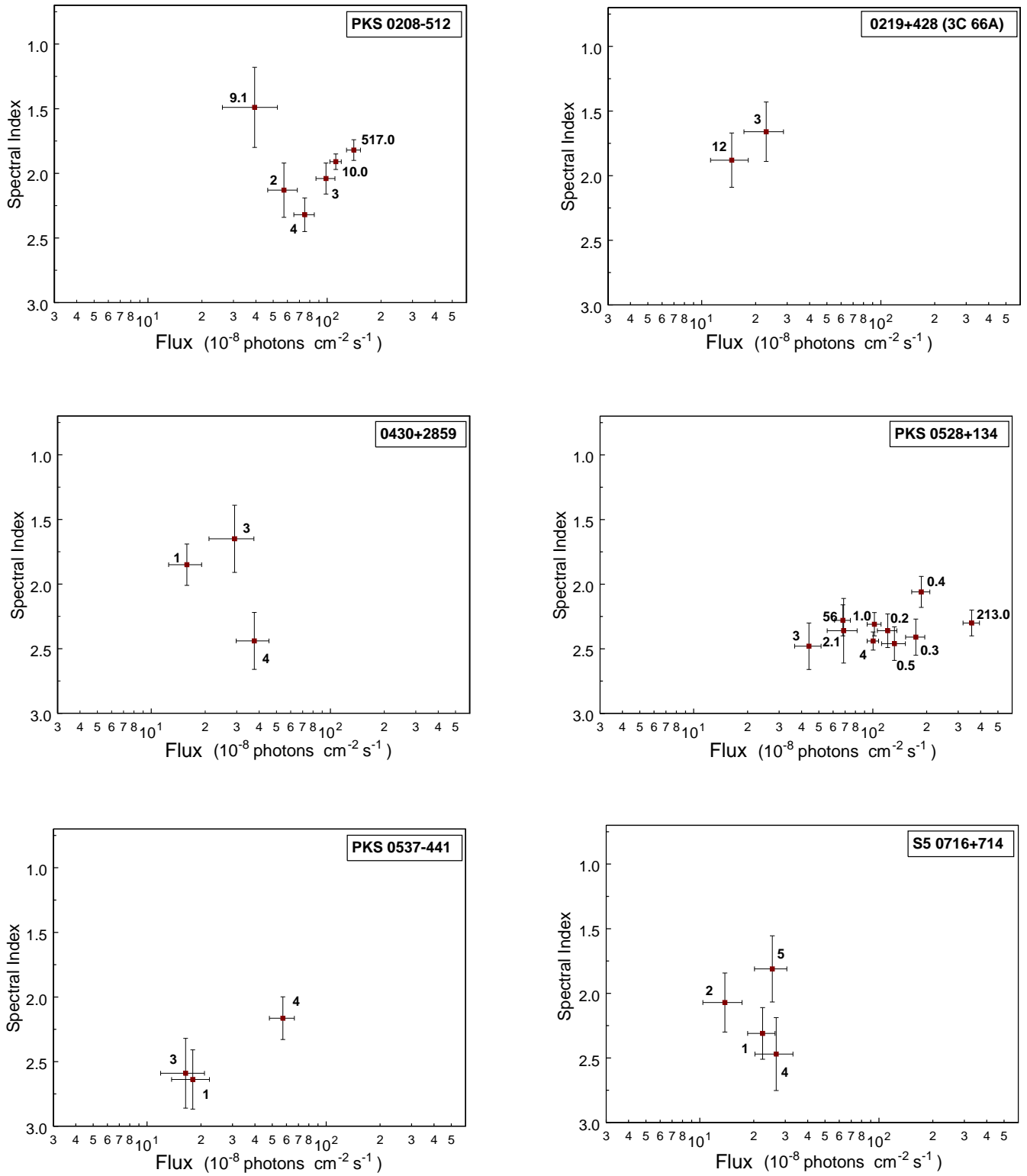
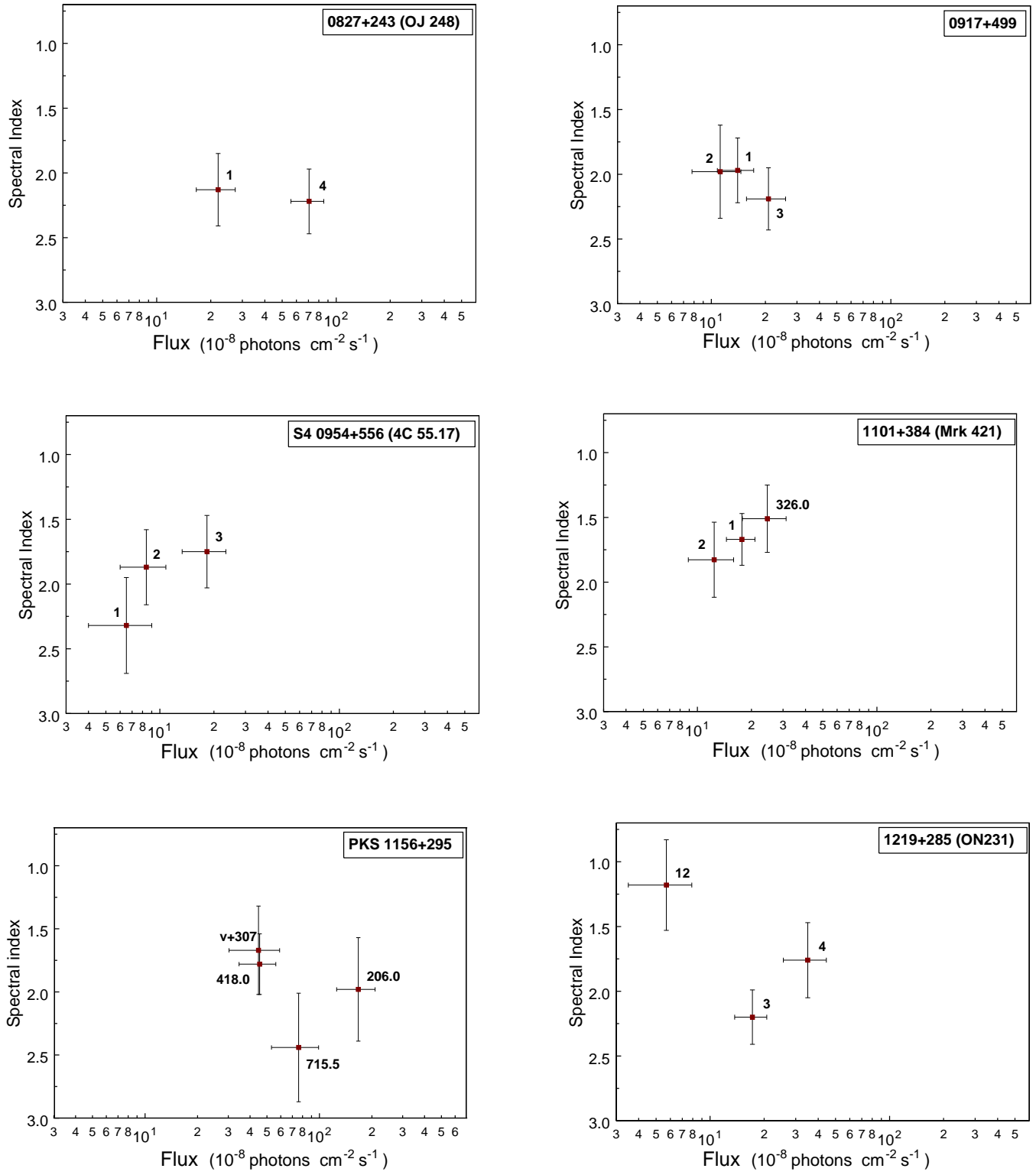
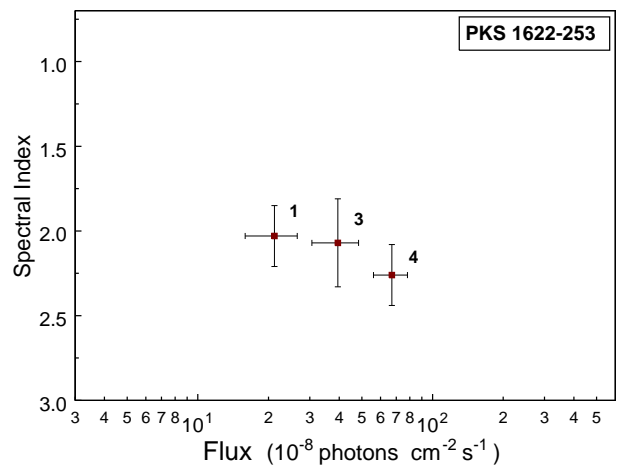
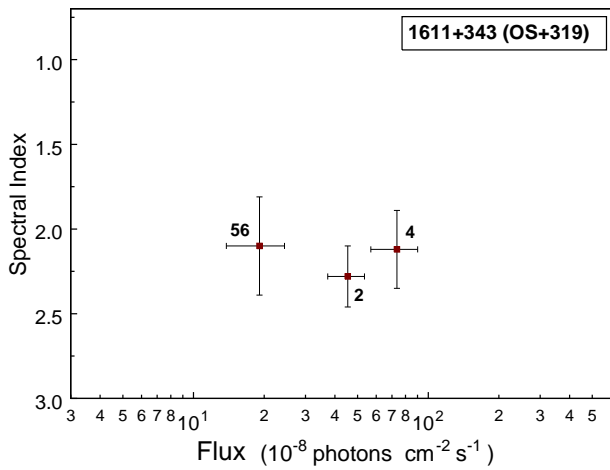
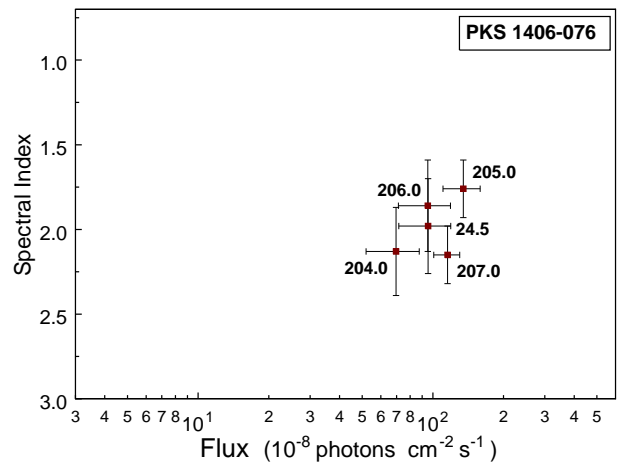
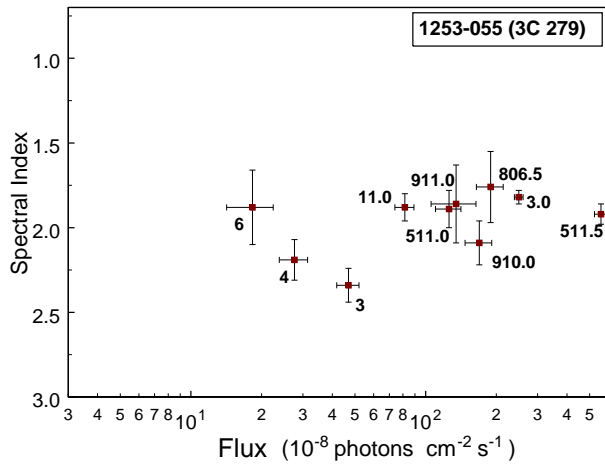
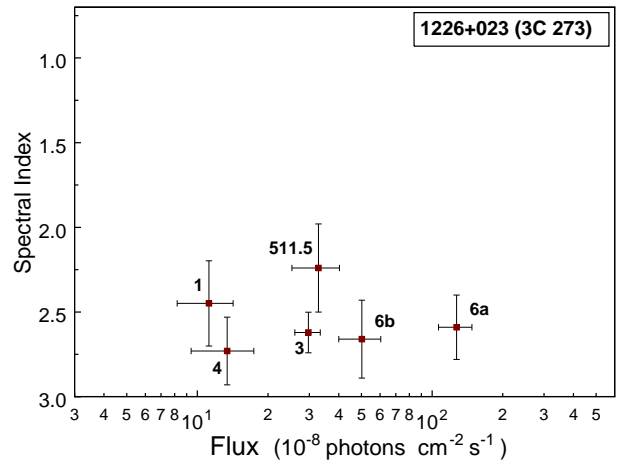
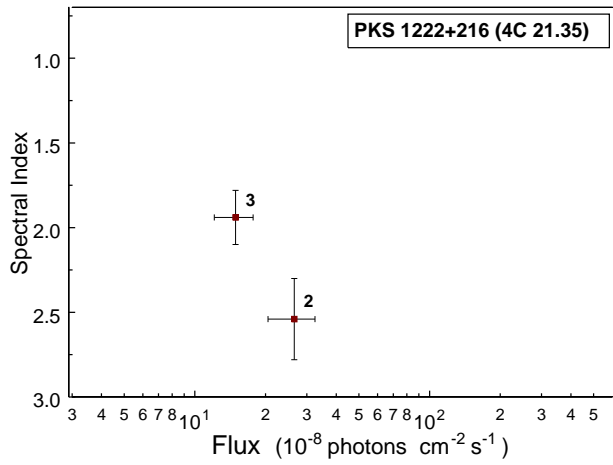
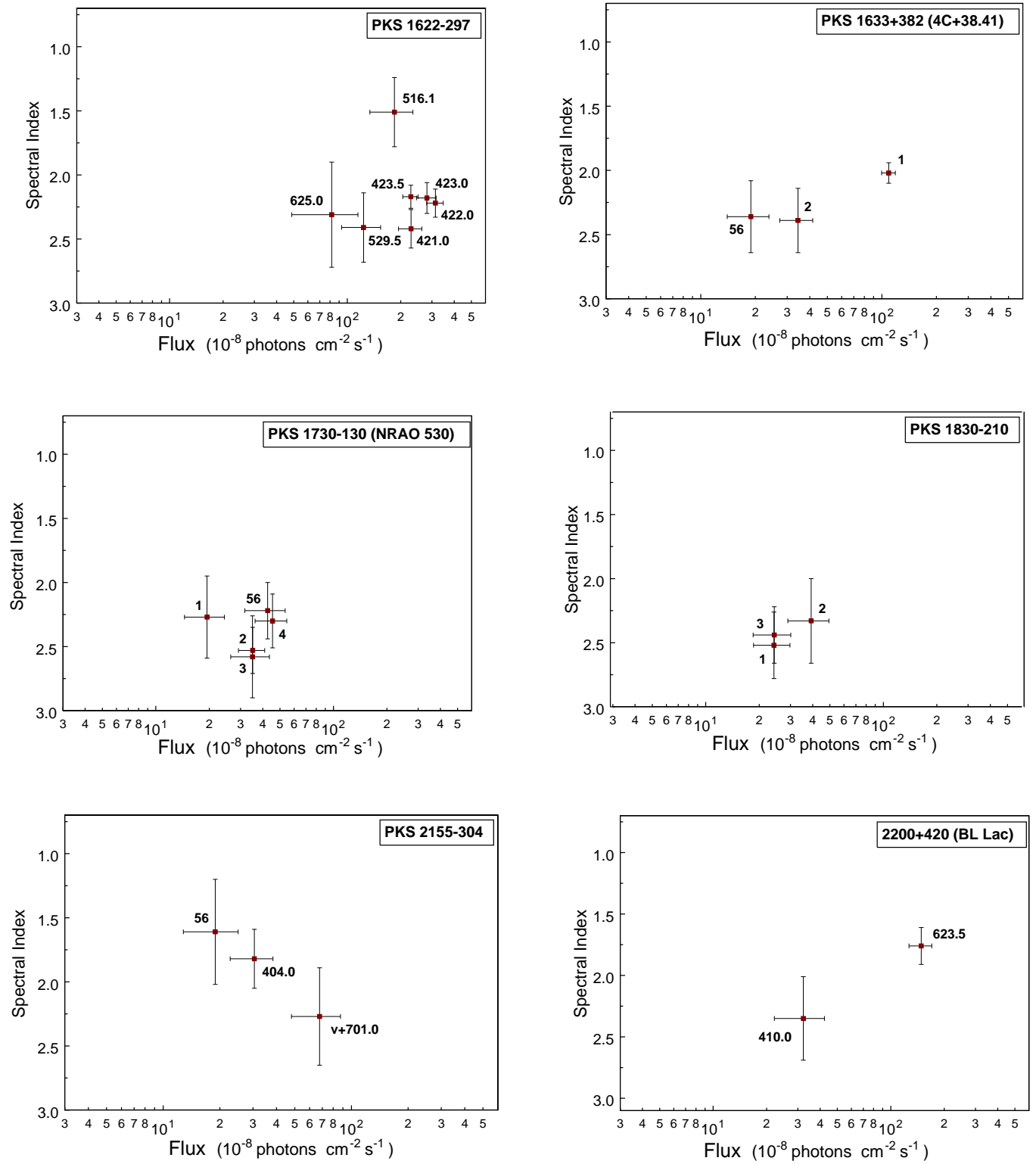
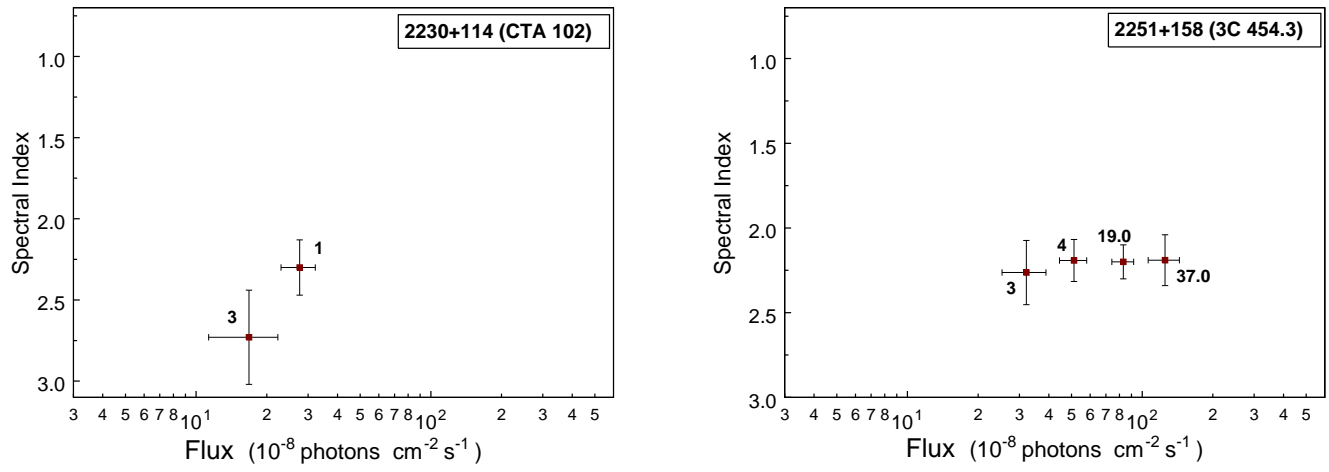


FIG. 3.— Variation of photon spectral index in the 30 MeV-10 GeV energy range with gamma-ray flux (>100 MeV) in units of 10^{-8} photons $\text{cm}^{-2} \text{s}^{-1}$. The spectral index is obtained from observations that are either one viewing period long (labeled by decimal numbers), or a combination of the viewing periods during one or more Cycle of observations (labeled by integers that show the Cycle(s) being combined). The details of the viewing periods/Cycles used in the analysis are given in Table 3.

FIG. 3.— *Continued*

FIG. 3.— *Continued*

FIG. 3.— *Continued*

FIG. 3.— *Continued*

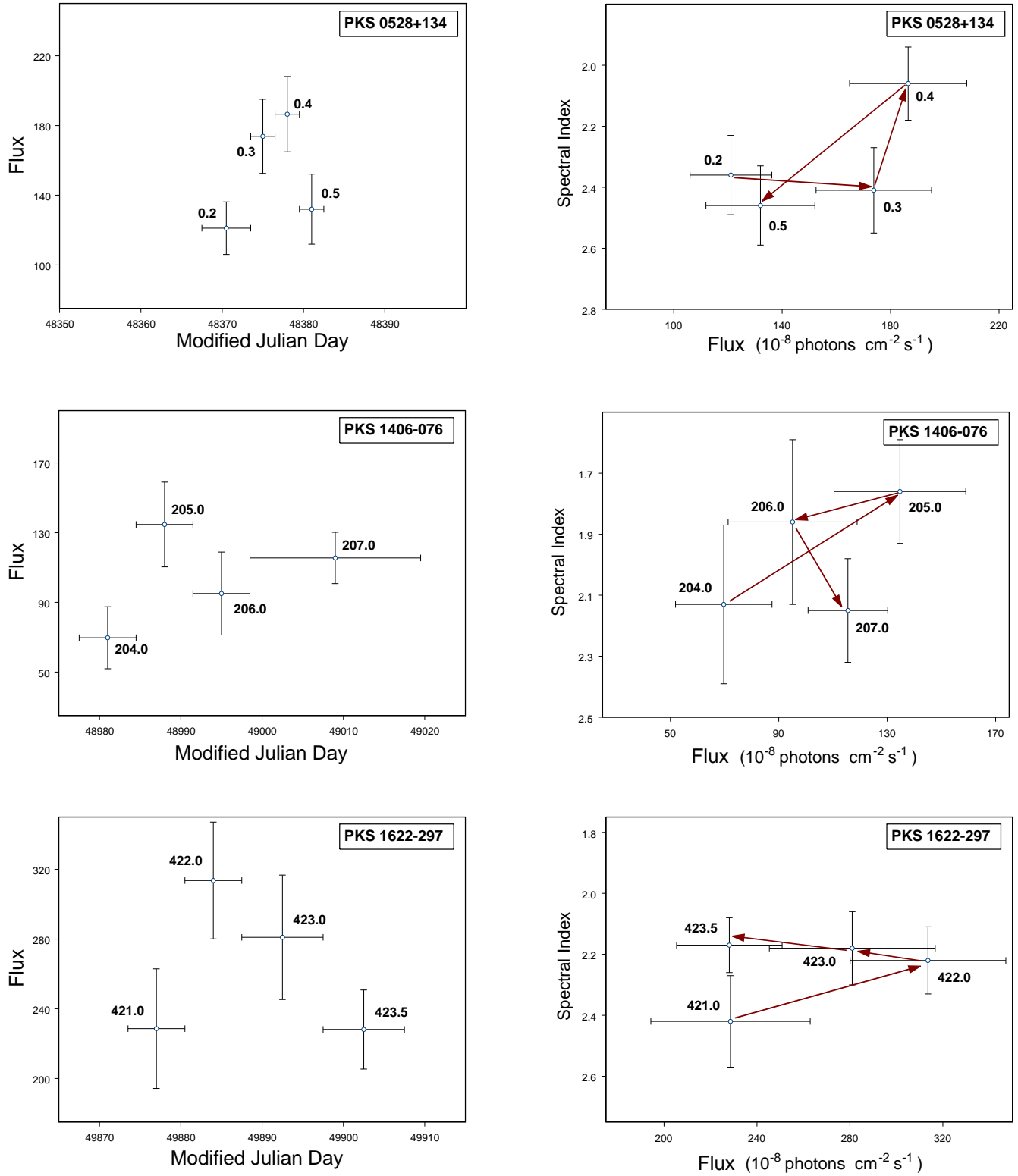


FIG. 4.— Spectral hysteresis during blazar flares that lasted 3–4 weeks. Graphs on the left show the variability of flux $> 100\text{MeV}$ in units of $10^{-8}\text{ photons cm}^{-2}\text{ sec}^{-1}$ with time (in MJD). The ranges for the time-axis and the flux axis are set to 50 days and 150 units respectively. The graphs on the right show hysteresis in the photon spectral index vs. flux space. The arrows show a chronological progression.

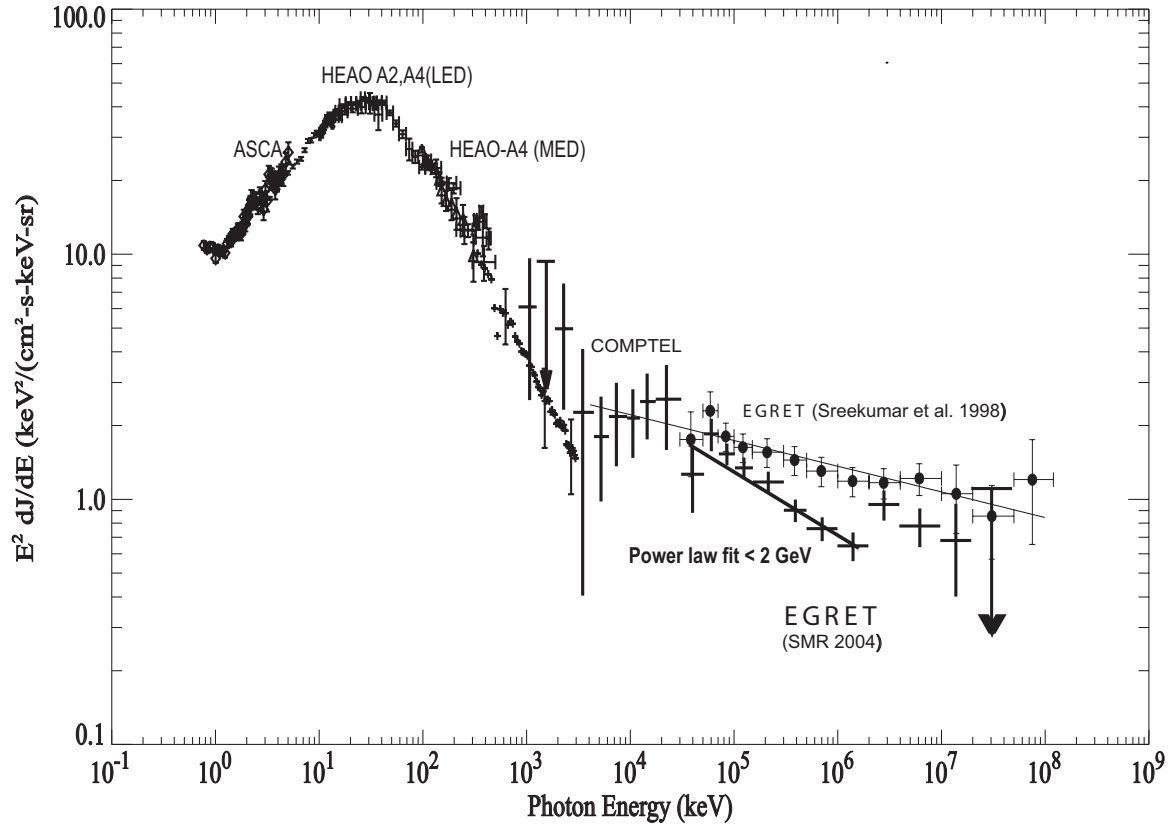


FIG. 5.— The X-ray and Gamma-ray background broadband spectrum. The data are taken from Strong et al. (2004). The extragalactic gamma-ray background (EGRB) calculated from the recalibrated EGRET data by Strong et al. (2004) (labeled SMR 2004) shows a break at 2 GeV and is steeper than the spectrum calculated by Sreekumar et al. (1998) in the energy range 30 MeV - 2 GeV. We were able to fit the points below 2 GeV with a power law of index 2.24 ± 0.01 , which is very close to the average blazar spectral index of 2.25 ± 0.03 obtained with the recalibrated EGRET data.

TABLE 1
 DETAILS OF THE VIEWING PERIODS(AFTER CYCLE 4) INCLUDED IN THE
 ANALYSIS AND THE SOURCES THAT WERE ANALYZED

Viewing Period ^a	Start Date	End Date	Sources	Viewing Angle ^b
502.0	10/17/95	10/31/95	PKS 0528+134	0.86
511.0	01/16/96	01/30/96	1253-055(3C 279)	6.72
511.5	01/30/96	2/06/96	1253-055(3C 279)	5.01
			1226+023(3C 273)	15.36
513.0	02/06/96	02/13/96	PKS 2155-304	0.16
515.0	02/20/96	03/05/96	1101+384(Mrk 421)	18.45
516.1	03/18/96	03/21/96	PKS 1622-297	10.91
516.5	03/21/96	04/03/96	PKS 1633+382(4C+38.41)	1.13
			PKS 1611+343(OS+319)	6.68
			Mrk 501	0.07
517.0	03/05/96	03/18/96	PKS 0208-512	2.25
518.5	04/03/96	04/23/96	S5 0716+714	0.00
519.0	04/23/96	05/07/96	PKS 1633+382(4C+38.41)	2.75
			PKS 1611+343(OS+319)	8.56
			Mrk 501	1.23
520.4	05/21/96	05/28/96	PKS 2155-304	0.00
526.0	07/30/96	08/13/96	PKS 0528+134	8.29
527.0	08/13/96	08/20/96	PKS 0528+134	9.27
528.0	08/20/96	08/27/96	PKS 0528+134	12.13
606.0	12/10/96	12/17/96	1226+023(3C 273)	11.34
			1253-055(3C 279)	1.00
607.0	12/17/96	12/23/96	1226+023(3C 273)	11.33
			1253-055(3C 279)	1.00
608.0	12/23/96	12/30/96	1226+023(3C 273)	11.24
			1253-055(3C 279)	1.01
609.0	12/30/96	01/07/97	1226+023(3C 273)	11.19
			1253-055(3C 279)	1.01
610.0	01/07/97	01/14/97	1226+023(3C 273)	11.19
			1253-055(3C 279)	1.01
610.5	01/14/97	01/21/97	1226+023(3C 273)	9.60
			1253-055(3C 279)	1.99
611.1	01/21/97	01/28/97	1226+023(3C 273)	11.16
			1253-055(3C 279)	1.01
616.1	02/18/97	03/18/97	PKS 0528+134	0.00
617.8	04/09/97	04/15/97	PKS 1633+382(4C+38.41)	6.71
			PKS 1611+343(OS+319)	12.57
			Mrk 501	2.99
621.5	06/17/97	06/24/97	1226+023(3C 273)	8.64
			1253-055(3C 279)	1.99
623.5	07/15/97	07/22/97	BL Lac	0.00
625.0	08/05/97	08/19/97	PKS 1622-297	17.68
615.1	08/19/97	08/26/97	PKS 1622-297	0.00
701.0	11/11/97	11/18/97	PKS 2155-304	4.92
708.0	12/30/97	01/06/98	PKS 2255-282	12.95
709.1	01/06/98	01/13/98	PKS 2255-282	12.95
715.5	03/20/98	03/27/98	PKS 1156+295	2.00
716.5	03/27/98	04/02/98	PKS 1156+295	17.98
806.5	01/19/99	01/26/99	1253-055(3C 279)	6.30
806.7	01/26/99	02/02/99	1253-055(3C 279)	2.87
910.0	02/08/00	02/23/00	1253-055(3C 279)	4.00
911.1	02/23/00	03/01/00	1253-055(3C 279)	8.40

^a EGRET was operated in the reduced field of view mode during all the viewing periods to conserve gas.

^b Viewing angle is in degrees

TABLE 2
 PHOTON SPECTRAL INDEX (30 MeV -10 GeV), AVERAGE FLUX (> 100 MeV)
 AND LOG(SYNCHROTRON PEAK FREQUENCY) OF BLAZARS DETECTED BY
 EGRET

Source	Possible(?)	Other names	RA ^a	DEC ^a	Spectral index ^b	Flux >100 MeV ^c	Log(ν_{sync}) ^d	Multiple Obs	Classification
0119+041	?	PKS, OC+033	19.60	2.81	2.24±0.34	12.6±4.3		N	FSRQ(HP)
0130-171	?	PKS	22.70	-17.97	2.37±0.29	12.4±3.8		N	FSRQ
0202+149		PKS	31.11	14.97	1.98±0.21	23.0±5.5	13±1	N	FSRQ(HP)
0208-512		PKS	32.58	-50.93	1.95±0.11	88.6±4.2	13.8±0.1	Y	FSRQ(HP)
0219+428		3C 66A	35.70	42.9	1.95±0.14	17.7±2.8	15.0±1.5	Y	LBL
0234+285	?	4C+28.07	39.99	28.26	2.56±0.23	12.7±2.9	13.5±1	N	FSRQ(HP)
0235+164		PKS, OD 160	39.36	16.59	1.86±0.11	25.4±3.6	13.3±0.3	N	LBL
0336-019		CTA 026	55.04	-2.02	1.87±0.22	15.5±3.5		N	FSRQ(HP)
0414-189			63.14	-18.88	1.96±0.45	44.2±15.5		N	FSRQ
0415+379	?	3C111	64.04	36.84	2.55±0.24	12.2±2.6		N	FSRQ
0420-014		PKS	65.65	-1.04	2.59±0.17	15.0±3.0	13.2±0.3	N	FSRQ(HP)
0430+2859	?		68.40	29.14	1.97±0.10	21.30±2.8	...	Y	LBL
0440-003		PKS, NRAO 190	70.55	-0.55	2.23±0.12	11.6±2.7	13.5±0.5	N	FSRQ(HP)
0446+112		PKS	72.61	11.09	2.19±0.15	14.0±2.0	13±1	N	FSRQ
0454-234		PKS	74.24	-23.64	2.27±0.32	7.5±2.5		N	LBL
0454-463		PKS	74.57	-46.60	2.56±0.37	7.8±2.1	13±1	N	FSRQ(LP)
0458-020	?	PKS	75.10	-1.99	2.45±0.22	10.2±2.2		N	FSRQ(HP)
0459+060	?		74.93	5.75	2.06±0.36	9.7±3.1		N	FSRQ
0506-612	?	PKS	78.15	-61.84	2.37±0.29	5.7±1.8		N	FSRQ
0521-365	?	PKS	82.54	-36.44	2.36±0.24	19.3±3.5	14.0±0.5	N	FSRQ(HP)
0528+134		PKS	82.74	13.38	2.36±0.03	95.8±3.7	13.0±0.2	Y	FSRQ(LP)
0537-286	?	PKS, OG-263	82.91	-29.68	2.23±0.50	32.6±11.5		N	FSRQ
0537-441		PKS	85.02	-44.05	2.36±0.12	24.3±3.0	13.5±0.5	Y	LBL
0539-057	?	PKS	85.57	-6.93	1.88±0.34	65.0±19.8		N	FSRQ
0616-116			95.58	-11.66	2.74±0.31	17.8±4.7		N	FSRS
0716+714		S5	110.43	71.35	2.19±0.11	18.4±2.1	15.0±0.1	Y	LBL
0735+178			114.47	17.35	2.44±0.23	14.8±3.1	14.5±0.5	N	LBL
0738+5451			115.83	54.80	2.00±0.19	11.1±2.1		N	FSRS
0803+5126	?		122.15	51.24	2.78±0.27	9.4±2.4		N	FSRQ
0805-077	?		123.14	-6.78	2.39±0.31	24.6±5.5	13.2±1	N	FSRQ
0804+499	?		122.18	48.75	2.13±0.42	9.9±2.4	13.5±1	N	FSRQ(HP)
OR 0809+483									
0827+243		OJ 248	127.49	24.22	2.38±0.2	25.4±3.9	13.3±1	Y	FSRQ(LP)
0829+046		OJ+049	127.03	5.14	2.42±0.42	16.1±4.9		N	LBL
0836+710		4C +71.07	131.46	70.83	2.69±0.16	9.7±1.7	13±0.5	N	FSRQ(LP)
0847-120			133.16	-12.27	1.48±0.26	44.4±11.8		N	FSRQ
0851+202		PKS, OJ 287	133.42	19.68	1.91±0.28	10.4±3.0		N	LBL
0917+449	?		139.33	44.45	2.06±0.14	14.1±2.1	13.0±0.5	Y	FSRQ(LP)
0954+556		4C 55.17	148.01	55.02	2.07±0.18	9.5±1.6	14.0±1.0	Y	FSRQ(HP)
0954+658		S4	149.62	65.56	2.03±0.18	6±1.6	13±1	N	LBL
1011+496	?		152.29	48.93	1.85±0.32	4.7±1.4		N	LBL
1055+567	?		163.21	57.31	2.15±0.37	9.0±2.4		N	LBL
1101+384		Mrk 421	166.10	38.15	1.57±0.14	13.6±1.8	16.7±0.5	Y	HBL
1127-145	?	PKS	173.66	-15.50	2.30±0.25	37.8±8.2	12.7±1	N	FSRQ(LP)
1156+295		PKS	180.12	28.80	1.97±0.17	8.7±1.8	14.5±0.3	Y	FSRQ(HP)
1219+285		PKS, W Comae, ON 231	185.75	28.70	1.80±0.17	11.5±1.5	14.5±0.5	Y	LBL
1222+216		4C 21.35	186.11	21.31	2.33±0.1	15.1±1.8	13±1	Y	FSRQ(LP)
1226+023		3C 273	185.25	2.17	2.56±0.07	19.5±1.7	13±1	Y	FSRQ(LP)
1229-021		PKS, 4C-02.55, ON-049	187.65	-2.79	2.64±0.36	5.5±1.5	13±1	N	FSRQ(LP)
1237+0459	?		188.91	4.97	2.78±0.32	4.8±1.5		N	FSRS
1243-072		PKS, ON-073	191.75	-6.86	2.75±0.17	8.4±1.9		N	FSRQ
1253-055		3C 279	193.98	-5.82	1.98±0.02	81.8±2.5	13.2±0.2	Y	FSRQ(HP)
1313-333	?	PKS, OP-322	198.51	-34.52	2.09±0.18	35.5±3.3	12.7±0.1	N	FSRQ
1322-428	?	PKS, Cen. A	201.15	-43.25	2.54±0.23	13.5±2.5		N	Radio Gal.
1324+224	?		200.80	22.01	1.62±0.24	17.9±4.1		N	FSRQ
1331+170		OP 151	202.39	17.14	2.38±0.38	7.6±2.6		N	FSRQ
1334-127		PKS	204.84	-14.32	1.92±0.25	11.9±3.3		N	FSRQ(HP)
1406-076		PKS	212.42	-7.75	2.21±0.10	31.3±3.0	14.8±0.2	Y	FSRQ(LP)
1424-418		PKS	217.39	-42.30	2.10±0.16	11.0±2.6	13.0±0.5	N	FSRQ(HP)
1504-166	?	PKS	226.20	-15.63	1.79±0.34	32.1±10.1		N	FSRQ
1510-089		PKS	228.17	-8.83	2.45±0.21	18.1±3.7	13.0±0.5	N	FSRQ(HP)
1514-241	?	PKS	229.34	-25.65	2.67±0.41	26.6±8.1		N	LBL
1604+159		4C+15.54	241.30	15.89	2.02±0.31	11.0±3.9	14±1	N	LBL
1606+106		4C 10.45	242.12	10.93	2.44±0.18	25.4±4.5	13.5±1	N	FSRQ(LP)
1611+343		OS+319	243.54	34.40	2.35±0.15	27.6±4.0		Y	FSRQ
1622-253		PKS	246.50	-25.32	2.12±0.14	24.2±3.5	12.5±1	Y	FSRQ(LP)
1622-297		PKS	246.36	-29.92	2.17±0.11	47.7±3.5	13.2±0.4	Y	FSRQ(LP)
1633+382		4C+38.41	248.92	38.22	2.15±0.08	59.±5.2	13±1	Y	FSRQ(LP)
1652+398		Mrk 501	253.47	39.76	1.48±0.44	10.1±4.1	18.5±1.0	N	HBL
1716-771	?		260.22	-78.34	2.08±0.47	19.8±6.9		N	FSRS
1725+044		PKS	261.97	4.50	2.63±0.26	16.2±3.9		N	FSRQ
1730-130		NRAO 530	263.46	-13.23	2.38±0.08	35.0 ± 3.3	13±1	Y	FSRQ

TABLE 2 — *Continued*

Source	Possible(?)	Other names	RA ^a	DEC ^a	Spectral index ^b	Flux >100 MeV ^c	Log(ν_{sync}) ^d	Multiple Obs	Classification
1739+522		4C+51.37	264.64	52.05	2.49±0.21	21.0 ±3.9	13±1	N	FSRQ
1741-038		PKS	266.02	-3.18	2.59±0.33	18.4 ±5.2	14±1	N	FSRQ(HP)
1759-396			270.22	-39.93	2.96±0.26	10.3±2.8		N	FSRS
1804-502	?	J1808-5011	271.55	-50.10	2.86±0.34	6.2±2.7		N	FSRS
1830-210			278.10	-21.18	2.62±0.13	26.6±3.6		Y	FSRQ
1908-201			287.93	-20.00	2.31±0.18	16.0±2.6		N	FSRS
1920-211	?		290.50	-20.26	2.37±0.48	28.3±8.0		N	FSRS
1933-400		PKS	293.98	-40.38	2.69±0.32	8.3±2.6	13.3±1	N	FSRQ
1936-155		PKS	294.47	-15.49	2.32±0.42	55.4±18.7		N	FSRQ
2002-233		TXS	301.54	-23.35	2.35±0.27	16.7±4.2		N	FSRS
2005-489	?	PKS	302.35	-48.83	...	11.0±4.4		N	HBL
2022-077			306.36	-7.75	2.32±0.17	20.0±3.5		N	FSRQ
2032+107		PKS	309.18	11.54	2.79±0.24	14.4±3.1	13.0±0.5	N	LBL
2052-474		PKS	313.80	-47.28	1.85±0.26	21.4±5.8	13.5±1	N	FSRQ(LP)
2105+598	?		315.18	60.21	2.07±0.24	19.4±4.1		N	FSRQ
2155-304		PKS	329.68	-30.40	1.88±0.17	18.8±2.9	16.2±0.2	Y	HBL
2200+420		BL Lac	330.60	42.29	1.72±0.18	20.3±3.2	14.6±0.4	Y	LBL
2206+650	?		331.60	66.05	2.37±0.25	25.9±5.2		N	FSRS
2209+236		PKS	332.41	24.03	2.31±0.32	13.3±4.2		N	FSRQ
2230+114		CTA 102	338.11	11.80	2.46±0.13	19.0±2.8	13±1	Y	FSRQ(HP)
2250+1926	?		343.99	19.73	1.87±0.43	62.2±22.2		N	FSRQ
2251+158		3C 454.3	343.51	16.02	2.22±0.06	56.5±4.0	13.5±0.5	Y	FSRQ(HP)
2255-282		PKS	344.52	-27.97	1.69±0.18 ^e	12.8±2.8	12.7±0.3	N	FSRQ(HP)
2320-035		PKS	350.41	-3.48	2.17±0.45	30.5±9.6		N	FSRQ
2346+385	?		358.10	37.88	2.70±0.33	35.5±10.2		N	FSRQ
2351+456			359.57	46.07	2.57±0.35	13.7±3.6		N	FSRQ
2356+196		OZ+193	359.99	20.70	2.24±0.33	8.5±2.8		N	FSRQ

NOTE. — FSRQ: Flat spectrum Radio Quasar; LBL: Low frequency-peaked BL Lac object; HBL: High frequency-peaked BL Lac object; HP: High polarization; LP: Low polarization; FSRS: Flat spectrum Radio Source. Classifications are based on Hartman et al. (1997) and Ghisellini et al. (1998)

^a These are EGRET positions from 3EG

^b Photon index measured in the 30 MeV - 10 GeV energy range

^c Flux is in units of 10^{-8} photons $\text{cm}^{-2} \text{s}^{-1}$

^d $\text{Log}(\nu_{sync})$ -Logarithm of the frequency (in Hz) of the synchrotron peak. These have been obtained from the literature cited in §4.1

^e Spectral index is during a flare. This was the only spectral index that could be calculated. The quoted flux is the average flux observed.

? Possible EGRET identification

TABLE 3
 GAMMA-RAY PHOTON SPECTRAL INDEX (30 MeV - 10 GeV) AND FLUX
 (>100MeV) OF BLAZARS THAT WERE BRIGHT AND WERE OBSERVED MULTIPLE
 TIMES BY EGRET. THE CORRESPONDING PLOTS OF SPECTRAL INDEX VS. FLUX
 ARE SHOWN IN FIG. 3.

Source	Start Dates	Viewing Periods Pooled	Graph label ^a in Fig. 3	Spectral Index (30 MeV-10 GeV)	Flux (> 100 MeV) ^c	Det. σ
0208-512	09/05/91	9.1	9.1	1.49±0.30	39.4±13.4	4.2
	09/19/91	10.0	10.0	1.91±0.06	111.8±8.2	21.5
	05/08/93, 06/03/93	220.0, 224.0	2	2.13±0.21	57.4±10.8	7.8
	05/31/94, 07/12/94, 07/25/94	329.0, 335.0, 335.5	3	2.04±0.12	98.6±12.0	6.7
	01/10/95, 09/07/95	409.0, 428.0	4	2.32±0.13	75.0±9.8	4.6
0219+428(3C 66A)	03/05/96	517.0	517.0	1.82±0.08	139.8±12.4	18.3
	11/28/91, 08/11/92, 08/12/92, 09/01/92, 02/25/93	15.0, 36.0, 36.5, 39.0, 211.0	12	1.88±0.21	14.7±3.5	4.9
	04/26/94	325.0	3	1.66±0.23	22.9±5.7	5.1
0430+2859	04/22/91, 04/28/91, 05/01/91, 05/04/91, 05/16/91, 06/08/91, 11/28/91, 06/11/92, 08/11/92, 08/12/92, 09/01/92	0.2, 0.3, 0.4, 0.5, 1.0, 2.1, 15.0, 31.0, 36.0, 36.5, 39.0	1	1.85±0.16	15.4±3.3	5.2
	12/01/93, 02/08/94, 02/15/94, 04/26/94	310.0, 321.1, 321.5, 325.0	3	1.65±0.26	25.8 ± 8.0	4.1
	02/28/95, 03/07/95, 05/23/95, 08/08/95, 08/22/95	412.0, 413.0, 420.0, 426.0, 427.0	4	2.44±0.22	37.6 ± 7.8	5.8
	04/22/91	0.2	0.2	2.36±0.13	121.0±15.1	10.4
0528+134	04/28/91	0.3	0.3	2.41±0.14	173.8±21.3	11.0
	05/01/91	0.4	0.4	2.06±0.12	186.5±21.6	12.0
	05/04/91	0.5	0.5	2.46±0.13	132.0±20.1	8.5
	05/16/91	1.0	1.0	2.31±0.09	102.1±9.1	14.5
	06/08/91	2.1	2.1	2.36±0.25	68.7±13.1	6.2
	03/23/93	213.0	213.0	2.30±0.10	356.7±37.7	14.0
	12/01/93, 02/08/94, 02/15/94, 08/09/94	310.0, 321.1, 321.5, 337.0	3	2.48±0.18	44.0±7.4	6.3
	02/28/95, 03/07/95, 04/04/95, 05/09/95,	412.0, 413.0, 419.1, 419.5, 420.0, 426.0	4	2.44±0.07	100.4±7.4	17.3
	10/17/95, 07/30/96, 08/13/96, 08/20/96, 02/18/97	502.0, 526.0, 527.0, 528.0, 616.1	56	2.28±0.12	68.1±6.9	11.7
	07/26/91, 08/22/91, 12/27/91, 05/14/92	6.0,8.0,17.0, 29.0	1	2.64±0.23	18.0±4.3	5.1
0537-441	05/31/94, 07/12/94, 07/25/94	329.0, 335.0, 335.5	3	2.59±0.27	16.4±4.5	4.5
	01/10/95, 04/11/95	409.0, 415.0	4	2.16±0.17	57.3±9.1	9.3
0716+714	05/07/91, 01/10/92, 03/05/92, 06/11/92	0.6, 18.0, 22.0, 31.0	1	2.31±0.20	22.4±3.9	7.3
	04/06/93, 04/06/93, 07/13/93	216.0, 227.0, 228.0	2	2.07±0.23	13.8±3.4	5.0
	03/01/94, 02/21/95	411.1, 411.5	4	2.47±0.28	26.7±6.4	5.4
0827+343 (OJ 248)	04/03/96, 09/06/96	518.5, 530.0	5	1.81±0.26	25.4±5.2	6.2
	09/17/92	40.0	1	2.13±0.28	22.0±5.4	5.2
0917+499	11/09/94	403.5	4	2.22±0.25	70.6±14.7	7.1
	05/07/91, 06/28/91, 01/10/92, 09/17/92	0.6, 4.0, 18.0, 40.0	1	1.97±0.25	14.0±3.2	5.5
0954+556 (4C 55.17)	04/06/93, 04/20/93, 05/24/93, 06/29/93, 07/13/93	216.0, 218.0, 222.0, 227.0, 228.0	2	1.98±0.36	11.2±3.40	4.1
	04/05/94, 05/10/94	322.0, 326.0	3	2.19±0.24	20.8±5.1	5.5
	05/07/91, 06/28/91, 01/10/92, 09/17/92	0.6, 4.0, 18.0, 40.0	1	2.32±0.37	6.50±2.5	3.1
	04/06/93, 04/20/93, 05/24/93, 06/29/93, 07/13/93	216.0, 218.0, 222.0, 227.0, 228.0	2	1.87±0.29	8.4±2.4	4.1
1101+384 (Mrk 421)	03/01/94, 03/15/94, 04/05/94 05/10/94	319.0, 319.5, 322.0, 326.0	3	1.75±0.28	18.3±5.0	4.8
	05/07/91, 06/28/91, 09/17/92	0.6, 4.0, 40.0	1	1.67±0.2	17.7±3.2	7.2
	04/20/93, 05/24/93, 06/29/93, 07/13/93	218.0, 222.0, 227.0, 228.0	2	1.83±0.29	12.4±3.5	4.6
1156+295	05/10/94	326.0	326.0	1.51±0.26	24.5±6.7	5.3
	01/05/93	206.0	206.0	1.98±0.41	166.9±41.4	6.8
	11/09/93, 11/16/93	307.0,308.0	v+307 ^b	1.67±0.35	44.7±14.4	4.1
1219+285 (ON 231)	04/25/95	418.0	418.0	1.78±0.24	45.4±10.8	6.3
	03/20/98	715.5	715.5	2.44±0.43	76.0±22.9	5.1
	06/15/91, 06/28/91, 10/03/91, 12/22/92, 12/29/92, 01/05/93, 04/20/93, 05/24/93	3.0, 4.0, 11.0, 204.0, 205.0, 206.0, 218.0, 222.0	12	1.18±0.35	5.7±2.2	3.0
	10/19/93, 10/25/93, 11/02/93, 11/09/93, 11/16/93, 11/23/93, 12/13/93, 12/17/93, 12/20/93, 12/27/93, 04/05/94, 05/10/94	304.0, 305.0, 306.0, 307.0, 308.0, 308.6, 311.0, 311.6, 312.0, 313.0, 322.0, 326.0	3	2.2±0.21	17.2±3.5	6.1
	12/13/94, 04/25/95	406.0, 418.0	4	1.76±0.29	35.0±9.4	4.9
	12/22/92, 12/29/92, 01/05/93, 04/20/93, 05/24/93	204.0, 205.0, 206.0, 218.0, 222.0	2	2.54±0.24	26.5±6.0	5.7

TABLE 3 — *Continued*

Source	Start Dates	Viewing Periods Pooled	Graph label ^a in Fig. 3	Spectral Index (30 MeV-10 GeV)	Flux (> 100 MeV) ^c	Det. σ
1226+023 (3C 273)	10/19/93, 10/25/93, 11/02/93, 11/09/93, 11/16/93, 11/23/93, 12/13/93, 12/17/93, 12/20/93, 12/27/93, 04/05/94, 05/10/94	304.0, 305.0, 306.0, 307.0, 308.0, 308.6, 311.0, 311.6, 312.0, 313.0, 322.0, 326.0	3	1.94±0.16	14.9±2.8	6.8
	06/15/91, 10/03/91	3.0, 11.0	1	2.45±0.25	11.2±3.0	4.3
	10/19/93, 10/25/93, 11/02/93, 11/09/93, 11/16/93, 11/23/93, 12/13/93, 12/17/93, 12/20/93, 12/27/93, 04/05/94, 05/10/94	304.0, 305.0, 306.0, 307.0, 308.0, 308.6, 311.0, 311.6, 312.0, 313.0, 322.0, 326.0	3	2.62±0.12	29.7±3.7	10.6
	11/29/94, 12/13/94, 12/20/94	405.0, 406.0, 407.0, 408.0	4	2.73±0.2	13.4±4.0	4.0
	01/03/95	511.5	511.5	2.24±0.26	32.8±7.5	5.8
	01/30/96	609.0, 610.0	6a	2.60±0.19	127.1±20.7	9.2
1253-055 (3C 279)	12/10/96, 12/17/96, 12/23/96, 01/14/97, 01/21/97	606.0, 607.0, 608.0, 610.5, 611.1	6b	2.66±0.23	50.2±10.2	6.60
	06/15/91	3.0	3.0	1.78±0.04	249.5±10.7	37.1
	10/03/91	11.0	11.0	1.88±0.08	81.5±7.6	15.2
	10/19/93, 10/25/93, 11/02/93, 11/09/93, 11/16/93, 11/23/93, 12/13/93, 12/17/93, 12/20/93, 12/27/93, 04/05/94, 05/10/94	304.0, 305.0, 306.0, 307.0, 308.0, 308.6, 311.0, 311.6, 312.0, 313.0, 322.0, 326.0	3	2.34±0.10	46.9±5.10	12.5
	11/29/94, 12/13/94, 12/20/94	405.0, 406.0, 407.0	4	2.19±0.12	27.6±3.8	9.2
	01/16/96	511.0	511.0	1.89±0.11	125.7±15.6	10.4
	02/20/96	511.5	511.5	1.92±0.06	558.6±34.5	27.6
	12/10/96, 12/17/96, 12/23/96, 12/30/96, 01/07/97, 01/14/97	606.0, 607.0, 608.0, 609.0, 610.0, 610.5	6	1.88±0.22	18.3±4.1	5.1
	01/21/97, 06/17/97	611.0, 621.5				
	01/19/99	806.5	806.5	1.76±0.21	189.2±24.8	9.6
1406-076	02/08/00	910.0	910.0	2.09±0.13	169.2±22.10	11.8
	02/23/00	911.1	911.1	1.87±0.24	134.7±29.2	7.0
	04/09/92	24.5	24.5	1.98±0.28	95.4±23.8	5.5
	12/22/92	204.0	204.0	2.13±0.29	69.7±17.8	5.5
	12/29/92	205.0	205.0	1.76±0.17	134.7±24.3	8.5
	01/05/93	206.0	206.0	1.86±0.27	95.1±23.1	6.1
	01/12/93	207.0	207.0	2.15±0.17	115.1±14.7	11.5
	11/17/92, 11/24/92	201.0, 202.0	2	2.28±0.18	45.4±8.1	7.7
	11/01/94	403.0	4	2.12±0.23	73.5±16.6	6.3
	03/21/96, 04/23/96, 04/09/97	516.5, 519.0, 617.8	56	2.10±0.29	19.1±5.3	4.6
1622-253	07/12/91, 12/12/91, 04/28/92, 09/09/93, 03/22/94, 04/19/94, 07/18/94, 08/04/94, 09/20/94	5.0, 16.0, 27.0, 302.3, 323.0, 324.0, 334.0, 336.5, 339.0	1 3	2.03±0.18 2.07±0.26	21.2±5.3 39.5±8.9	4.4 4.5
	06/06/95, 06/13/95, 06/20/95, 06/30/95	421.0, 422.0, 423.0, 423.5	4	2.26±0.18	67.10±11.10	7.9
	06/06/95	421.0	421.0	2.42±0.15	228.6±34.30	9.3
1622-297	06/13/95	422.0	422.0	2.22±0.11	313.6±33.50	14.3
	06/20/95	423.0	423.0	2.18±0.12	281.0±35.7	11.2
	06/30/95	423.5	423.5	2.17±0.09	228.1±22.7	14.9
	03/18/96	516.1	516.1	1.51±0.27	184.2±50.2	5.3
	08/27/96	529.5	529.5	2.41±0.27	123.6±30.6	5.3
	08/05/97	625.0	625.0	2.31±0.42	81.8±33.1	3.3
1633+382 (4C +38.41)	09/12/91	9.2	1	2.02±0.08	109.1±9.5	17.8
	11/17/92, 11/24/92	201.0, 202.0	2	2.39±0.25	34.4±7.1	6.4
	03/21/96, 04/23/96, 04/09/97	516.5, 519.0, 617.8	56	2.36±0.8	18.9±4.9	4.7
1730-130 (NRAO 530)	07/12/91, 08/15/91, 10/31/91	5.0, 7.2, 13.1	1	2.27±0.32	19.40±4.9	4.4
	12/12/91, 02/06/92, 02/22/93, 03/29/93, 05/05/93	16.0, 20.0, 210.0, 214.0, 219.0	2	2.58±0.32	35.0±8.6	4.6
	05/31/93, 06/19/93, 08/03/93	223.0, 226.0, 231.0				
	08/10/93, 08/12/93, 08/24/93	229.0, 229.5, 232.0				
	09/09/93, 03/22/94, 04/19/94	302.3, 323.0, 324.0	3	2.53±0.18	35.1±5.9	6.8
	06/10/94, 06/18/94, 07/18/94	330.0, 332.0, 334.0				
1830-210	06/06/95, 06/13/95, 06/20/95, 06/30/95, 09/20/95	421.0, 422.0, 423.0, 423.5, 429.0	4	2.47±0.09	34.1±3.3	11.8
	07/12/91, 08/15/91, 10/31/91, 12/12/91, 02/06/92	5.0, 7.2, 13.1, 16.0, 20.0	1	2.52±0.26	24.2±5.6	4.6
	02/22/93, 03/29/93, 05/31/93, 06/19/93, 08/03/93	210.0, 214.0, 223.0, 226.0, 231.0	2	2.33±0.33	39.2±10.2	4.3
	08/10/93, 08/12/93, 08/24/93	229.0, 229.5, 232.0				
	09/09/93, 03/22/94, 04/19/94	302.3, 323.0, 324.0	3	2.44±0.22	24.3±5.8	4.6
	06/10/94, 06/18/94, 07/18/94	330.0, 332.0, 334.0				
2155-304	11/15/94	404.0	404.0	1.82±0.23	30.5±7.8	5.9
	02/06/96, 05/21/96	513.0, 520.4	56	1.61±0.41	18.9±6.0	4.1
	11/11/97, 11/18/97	701.0, 702.0	v+701.0 ^b	2.27±0.38	67.7.0±19.7	4.9
2200+420 (BL Lac)	01/24/95	410.0	410.0	2.35±0.34	32.2±10.10	4.0
	07/15/97	623.5	623.5	1.76±0.15	148.4±21.7	10.2

TABLE 3 — *Continued*

Source	Start Dates	Viewing Periods Pooled	Graph label ^a in Fig. 3	Spectral Index (30 MeV-10 GeV)	Flux (> 100 MeV) ^c	Det. σ
2230+114 (CTA 102)	01/23/92, 04/23/92, 05/07/92, 08/20/92	19.0, 26.0, 28.0, 37.0	1	2.30±0.17	27.60±4.60	7.9
2251+158 (3C 454.3)	03/08/94, 05/17/94, 08/01/94	320.0, 327.0, 336.0	3	2.73±0.29	16.8±5.5	3.3
	01/23/92	19.0	19.0	2.20±0.10	83.1±8.9	13.5
	08/20/92	37.0	37.0	2.19±0.15	125.1±19.0	10.0
	03/08/94, 05/17/94, 08/01/94	320.0, 327.0, 336.0	3	2.26±0.19	32.1±6.8	5.9
	01/24/95	410.0	4	2.19±0.12	51.2±6.8	10.9

^a The label used to identify each point in the spectral index vs. flux plots shown in Fig. 3. The labels are represented by a decimal number if the data is from a single viewing period, and an integer if the data from one or more EGRET Cycle(s) is combined.

^b Any label starting with v+ indicates a combination of only a fraction of the viewing periods during a cycle. The source was comparatively faint during the other viewing periods of the cycle.

^c Flux is in units of 10^{-8} phot. $\text{cm}^{-2} \text{s}^{-1}$

TABLE 4
SPECTRAL VARIABILITY RESULTS. COLUMNS 3, 4 & 5 ARE RESULTS FROM THE χ^2 TEST AND COLUMN 5 LISTS THE CORRELATION COEFFICIENT BETWEEN GAMMA-RAY SPECTRAL INDEX AND FLUX (> 100 MeV). THE COEFFICIENT IS NEGATIVE WHEN THE SPECTRAL INDEX (POSITIVE) HARDENS WITH INCREASING FLUX.

Source	Mean \pm Stdev ($\Gamma_\mu \pm \sigma$)	χ^2_{red}	DOF ^b	Confidence Level (%) of variability	Pearson's Corr. Coeff
0208-512	1.95 \pm 0.28	2.93	5	99	+0.10
0219+428 (3C 66A)	1.77 \pm 0.16	0.50	1	52	^a
0430+2859	1.98 \pm 0.41	3.32	2	97	+0.62
0528+134	2.36 \pm 0.12	1.10	9	62	-0.34
0537-441	2.46 \pm 0.26	2.04	2	87	-0.99
0716+714	2.17 \pm 0.29	1.25	3	71	+0.21
0827+243 (OJ 248)	2.17 \pm 0.06	0.06	1	19	^a
0917+499	2.05 \pm 0.12	0.24	2	21	+0.95
0954+556 (4C 55.17)	1.98 \pm 0.3	0.83	2	56	-0.77
1101+384 (Mrk 421)	1.67 \pm 0.16	0.34	2	28	-0.99
1156+295	1.97 \pm 0.34	0.85	3	53	+0.28
1219+285 (ON 231)	1.71 \pm 0.51	3.86	2	98	+0.46
1222+216 (4C 21.35)	2.24 \pm 0.42	5.07	1	98	^a
1226+023 (3C 273)	2.55 \pm 0.17	0.60	5	31	+0.11
1253-055 (3C 279)	1.98 \pm 0.18	3.9	9	100	-0.32
1406-076	1.98 \pm 0.17	0.79	4	46	-0.54
1611+343 (OS+319)	2.16 \pm 0.10	0.24	2	22	+0.08
1622-253	2.12 \pm 0.12	0.44	2	36	+0.97
1622-297	2.17 \pm 0.31	1.63	6	87	-0.07
1633+382 (4C+38.41)	2.25 \pm 0.20	4.59	2	99	-0.97
1730-130 (NRAO 530)	2.42 \pm 0.16	0.47	4	24	-0.05
1830-210	2.43 \pm 0.10	0.1	2	10	-0.91
2155-304	1.88 \pm 0.30	0.78	2	54	+0.99
2200+420 (BL Lac)	1.94 \pm 0.25	1.75	1	81	^a
2230+114 (CTA 102)	2.51 \pm 0.30	2.15	1	86	^a
2251+158 (3C 454.3)	2.22 \pm 0.03	0.04	3	1	-0.69

^a Correlation coefficient was not determined since the sample size was less than 3

^b The DOF (degrees of freedom) is for the χ^2 test of variability and is one less than the sample size.